Adv Compos Hybrid Mater (2018) 1:56–78
DOI 10.1007/s42114-017-0004-3

REVIEW

Carbon nanotubes, graphene, and their derivatives for heavy metal removal

Guoqiang Yu[1] · Yang Lu[2] · Jiang Guo[3] · Manisha Patel[1] · Adarsh Bafana[1] · Xifan Wang[4] · Bin Qiu[5] · Clayton Jeffryes[1] · Suying Wei[6] · Zhanhu Guo[3] · Evan K. Wujcik[1,2,7,8]

Received: 7 March 2017 / Revised: 16 April 2017 / Accepted: 26 April 2017 / Published online: 25 September 2017

Abstract Carbon nanoadsorbents have attracted tremendous interest for metal ion removal from wastewater due to their extraordinary aspect ratios, surface areas, porosities, and reactivities. However, challenges still exist as they suffer from subpar dispersion and recovery, tending to aggregate, and so on. Thus, significant research efforts focus on modification of these carbon nanomaterials to increase the dispersions and recoveries, while maintaining or even enhancing the desirable properties. This review aims to give an in-depth look at recent and impactful advances in metal ion adsorption applications involving these modified carbon nanostructures. Here, the advanced design and testing of modified carbon nanostructures for metal ion removal are emphasized with comprehensive examples, and various adsorption behaviors and mechanisms are discussed, which are hoped to help the development of more effective adsorbents for water treatment.

Keywords Carbon nanoadsorbents · Heavy metals · Water treatment · Modification methods · Adsorption behaviors

1 Introduction

Industrial, agricultural, and domestic activities inevitably produce large amounts of wastewater [1–3]. Pollutants in the water can mainly be divided into three categories: microorganisms, organics, and inorganics. Heavy metal ions, as the major part of inorganic pollutants, have aroused lots of concern due to their toxicities to ecological and biological systems [4–8]. The United States Environmental Protection Agency (EPA) has limited the levels of various metal ions in drinking water. Table 1 lists some of them and the corresponding effects on human health [9].

Water pollution due to metal ions is still a serious problem and great challenge throughout the world. A tremendous amount of research focuses on this area, and many methods have been developed, such as adsorption [10, 11], ion exchange [12, 13], membrane filtration [14, 15], electrochemical precipitation [16, 17], reverse osmosis [18, 19], and flocculation [20, 21]. Among these methods, adsorption is most widely used to remove metal ions from wastewater

✉ Suying Wei
Suying.Wei@lamar.edu

✉ Zhanhu Guo
zguo10@utk.edu

✉ Evan K. Wujcik
Evan.Wujcik@ua.edu

[1] Dan F. Smith Department of Chemical Engineering, Lamar University, Beaumont, TX, USA

[2] Materials Engineering And Nanosensor (MEAN) Laboratory, Department of Chemical and Biological Engineering, The University of Alabama, Tuscaloosa, AL, USA

[3] Integrated Composites Laboratory (ICL), Department of Chemical & Biomolecular Engineering, University of Tennessee, Knoxville, TN, USA

[4] Department of Materials Science and NanoEngineering, Rice University, Houston, TX, USA

[5] College of Environmental Science & Engineering, Beijing Forestry University, Beijing, People's Republic of China

[6] Department of Chemistry and Biochemistry, Lamar University, Beaumont, TX, USA

[7] Department of Materials Science, The University of Alabama, Tuscaloosa, AL, USA

[8] Center for Materials for Information Technology [MINT], The University of Alabama, Tuscaloosa, AL, USA

Table 1 EPA maximum contaminant levels in drinking water and corresponding health effects

Metal	MCL (ppb)[a]	Health effects
Arsenic (As)	10	Skin damage or circulatory system problems, cancer risk may increase
Cadmium (Cd)	5	Kidney damage
Chromium (Cr)	100	Allergic dermatitis
Copper (Cu)	1300	Gastrointestinal distress, liver or kidney damage
Lead (Pb)	15	Deficits in attention span and learning abilities, kidney problems, blood pressure increases
Mercury (Hg)	2	Kidney damage
Uranium (U)	30	Cancer risk increases, kidney toxicity

[a] MCL: maximum contaminant level; ppb: parts per billion, 1 ppb = 1 μg/L.

due to its simple, economical, and highly efficient characteristics [22, 23]. Lots of adsorbents including carbon materials [24, 25], metal oxides [26, 27], clays [28, 29], zeolites [30, 31], biomass [32, 33], and polymers [34, 35] have been explored.

Carbon nanomaterials, some of which are shown in Fig. 1, are the most commonly employed adsorbents for metal ion removal from wastewater owing to their large specific surface area and concentrated pore distribution [36, 37]. Moreover, they exhibit a great mechanical property and excellent structural stability under extreme conditions (e.g., high temperature and strong acidic/alkaline conditions) [38–40]. However, it is often difficult to disperse them in an aqueous environment and recover them after adsorption due to their hydrophobicity and small size [41–43]. In addition, some carbon nanomaterials, such as graphene, tend to aggregate decreasing their surface area and surface energy, which strongly decreases their adsorption performance [44–46]. To overcome these disadvantages, much attention has been paid to decorating the carbon nanomaterials. Various modified carbon nanoadsorbents have been developed because of the widespread functionalization of carbon nanomaterials.

In this review, the uses of modified carbon nanoadsorbents for metal ion removal from water are focused on. Different types of carbon-based nanoadsorbents and their adsorption performances, common methods to modify carbon nanomaterials, various adsorption isotherm and kinetic models, diverse adsorption mechanisms, and practical applications of the modified carbon nanoadsorbents to environmental water samples are covered. Furthermore, some issues about current research are discussed. For example, the adsorbents with such characteristics as high selectivity, extreme sensitivity, or none toxicity are rarely reported. It is hoped that this review can help to promote the development of carbon-based nanoadsorbents and the treatment for water pollution.

2 Overview

Based on their different architectures, carbon nanomaterials include zero-dimensional carbon nanoparticles and carbon nanospheres, one-dimensional carbon nanotubes (CNTs) and carbon nanofibers, two-dimensional graphene and carbon nanofabrics, and three-dimensional carbon nanoclusters and carbon nanofoams. A variety of adsorbents involving them are thus developed.

2.1 Graphene-based nanoadsorbents

Graphene possesses a two-dimensional structure consisting of sp^2 hybridized carbon atoms covalently bonded in a honeycomb or hexagonal lattice with only one atomic thickness [47–50]. Due to its superior thermal, mechanical, electronic, and chemical properties, graphene and its derivatives can be applied to many fields, such as electronics, energy, sensors, and composites [51–54]. Moreover, since it has a huge surface area, large delocalized π-electron system, and tunable chemical properties, graphene and its derivatives can be used to effectively adsorb metals from wastewater [55–57]. Graphene as the nanoadsorbent mainly includes three forms: pristine graphene, graphene oxide (GO), and reduced graphene oxide (rGO) [58]. GO is an oxidized form of graphene, containing various oxygen-containing groups, such as epoxide, carbonyl, carboxyl, and hydroxyl groups [59–63]. Since the oxygen groups break the double bonds holding the carbon atoms together, GO loses its electrical conductivity. However, these oxygen groups cause GO to become polar and easy to disperse in water [64–66]. rGO is the reduction product of GO, which can be prepared through thermal, chemical, or electrical treatments of GO. Compared to pristine graphene, rGO contains more such defects as residual oxygen and other heteroatoms and has a lower conductivity.

Xu et al. [67] successfully prepared polyacrylamide grafted graphene (PAM-g-graphene) through γ-ray treatment of graphite oxide and acrylamide, which was characterized by UV-Vis absorption spectroscopy, XRD, XPS, FTIR, TGA, and AFM. The as-prepared PAM-g-graphene had a thickness of 2.59 nm, N_2-BET-specific surface area of 128 m^2/g, and grafted PAM chains of 24.2 wt%. In contrast, the N_2-BET specific surface area of pristine graphite oxide and the thickness of its single-layer sheets were 46.4 m^2/g and 1.30 nm, respectively. A superior performance for Pb(II) adsorption was exhibited by the PAM-g-graphene. Figure 2 a, b shows that the adsorption equilibrium could be reached in 30 min, and the adsorption kinetics was well described by the pseudo-

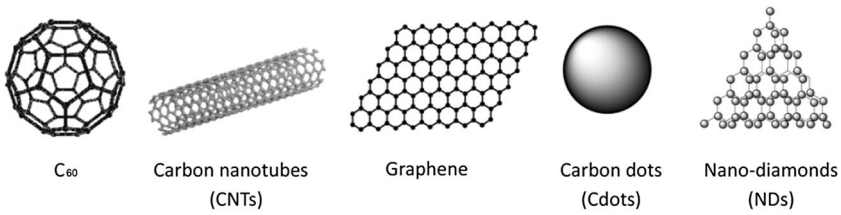

Fig. 1 Some carbon nanostructures. Reprinted with permission from Ivyspring International Publisher [36]

second order model. Langmuir and Freundlich isotherm models were employed to illustrate the adsorption isotherms, as shown in Fig. 2 c, d. The maximum adsorption capacity determined by the Langmuir isotherm model was 819.67 mg/g, which was respectively 20 times and 8 times higher than that of graphene nanosheets and CNTs. The one-step synthesis of PAM-g-graphene exhibited a bright prospect for heavy metal removal from water.

As shown in Fig. 3, L-cystine functionalized exfoliated GO (EGO) was synthesized and used for Hg(II) adsorption [68]. First, graphite was oxidized and exfoliated to prepare GO. Then GO was treated with thionyl chloride ($SOCl_2$), and acylchloride groups were formed due to the reaction between carboxyl groups of the GO and $SOCl_2$. After that, L-cystine was added, and its amine groups reacted with acylchloride groups to produce acylamide groups. In this way, L-cystine was successfully grafted onto EGO. Nitrogen, oxygen, and sulfur-containing groups on the L-cystine functionalized EGO could effectively bind Hg(II), and an outstanding adsorption performance was observed. Compared with unmodified graphite, L-cystine functionalized EGO had a much higher adsorption capacity under the same conditions, which were 79.36 and 12.4 mg/g, respectively. Moreover, there was no significant interference from other metal ions when they were at low concentrations. Thiourea could be employed to accelerate the process of desorption, and after four adsorption-desorption cycles, the adsorption efficiency began to decrease.

Radionuclides can cause serious environmental problems. Wen et al. [69] prepared three-dimensional hierarchical flower-like GO-hydroxyapatite (GO-HAp) nanocomposites for Sr(II) removal. The GO was synthesized through a modified Hummers method, and the HAp grew on the GO nanosheets via a biomimetic method. The process of HAp nucleation and growth was shown in Fig. 4. To evaluate the adsorption ability of GO-HAp, effects of contact time, solution pH, coexisting cations, GO-HAp content, and Sr(II) initial concentrations were investigated. The adsorption equilibrium could be quickly reached within 2 h, and the removal kinetics followed the pseudo-second-order model. The GO-HAp

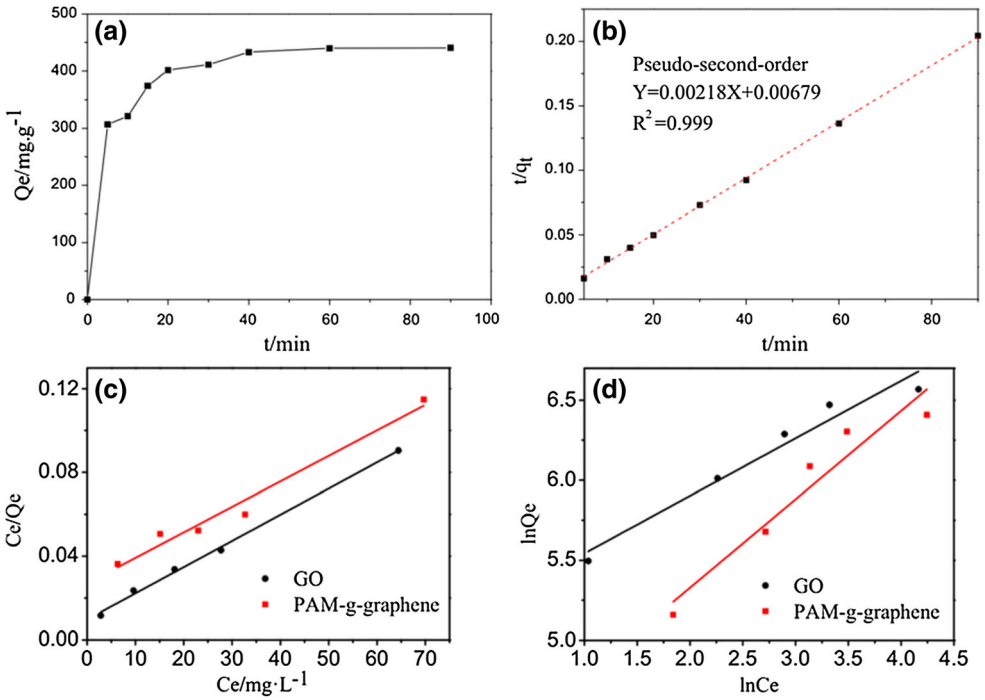

Fig. 2 **a** Effect of the contact time on the adsorption of Pb(II) onto PAM-g-graphene (adsorbent 0.1 g/L; initial Pb(II) concentration 45 mg/L; pH 6; *T* 293 K); **b** adsorption kinetics of Pb(II) onto PAM-g-graphene fitted by pseudo-second-order model; adsorption isotherm of Pb(II) onto PAM-g-graphene fitted by **c** Langmuir model and **d** Freundlich model (adsorbent 0.1 g/L; initial Pb(II) concentration 5–100 mg/L; pH 6; *T* 293 K). Reprinted with permission from Elsevier [67]

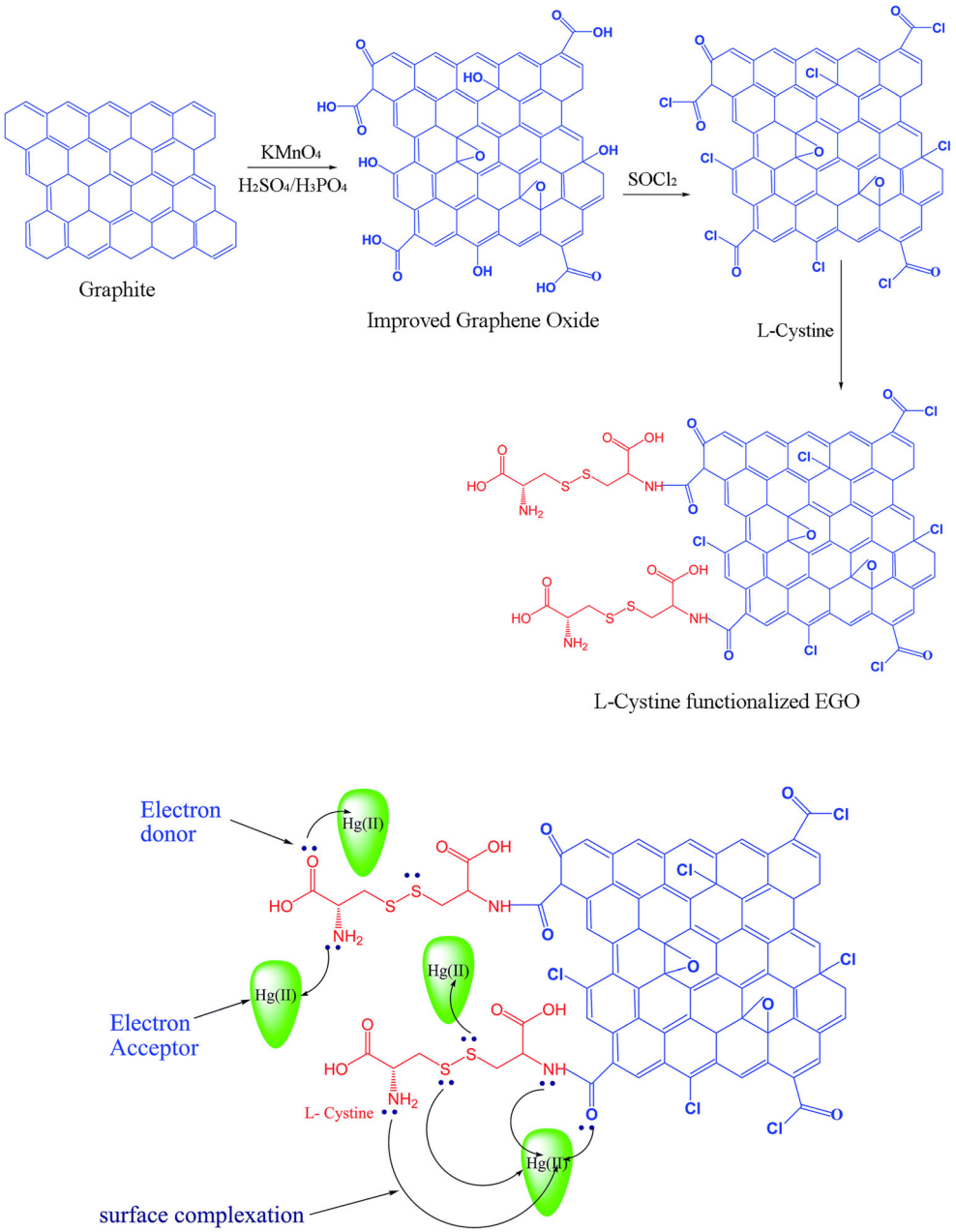

Fig. 3 Preparation process of L-cystine functionalized EGO and its interactions with Hg(II). Reprinted with permission from Royal Society of Chemistry [68]

could keep a high removal percentage in a wide pH range, more than 76% even at pH 2–4. Cd(II) and Pb(II) had a slight influence on the adsorption of Sr(II), while Mg(II), Al(III), and Na(I) had almost no effects. As more GO-HAp were added to the solution, the adsorption percentage of Sr(II) increased swiftly, whereas its distribution coefficient gradually decreased. Both the Langmuir and Freundlich isotherms could well describe the adsorption behaviors of Sr(II). A maximum adsorption capacity of 702.18 mg/g was obtained from the Langmuir model, which was higher than most other adsorbents, almost two times that of bare HAp and nine times that of GO. Two possible mechanisms for Sr(II) adsorption were proposed, namely ion exchange between Ca(II) and Sr(II) and complex compound formation of Sr(II) with HAp active surface sites. The GO-HAp showed great potential applications for radiostrontium pollution clean-up.

Yang et al. [70] employed a new adsorbent, lignosulfonate-GO-polyaniline (LS-GO-PANI) ternary nanocomposite, to adsorb Pb(II) from water. GO was first fabricated from expansible graphite via an airtight oxidation method, and then LS-GO-PANI was prepared through an in situ polymerization of aniline in the presence of LS and GO in a HCl aqueous solution, as shown in Fig. 5. Compared with PANI and GO-PANI, LS-GO-PANI ternary nanocomposite exhibited a higher adsorption capacity due to the existence of a synergistic effect among the functional groups on it. It was believed that the

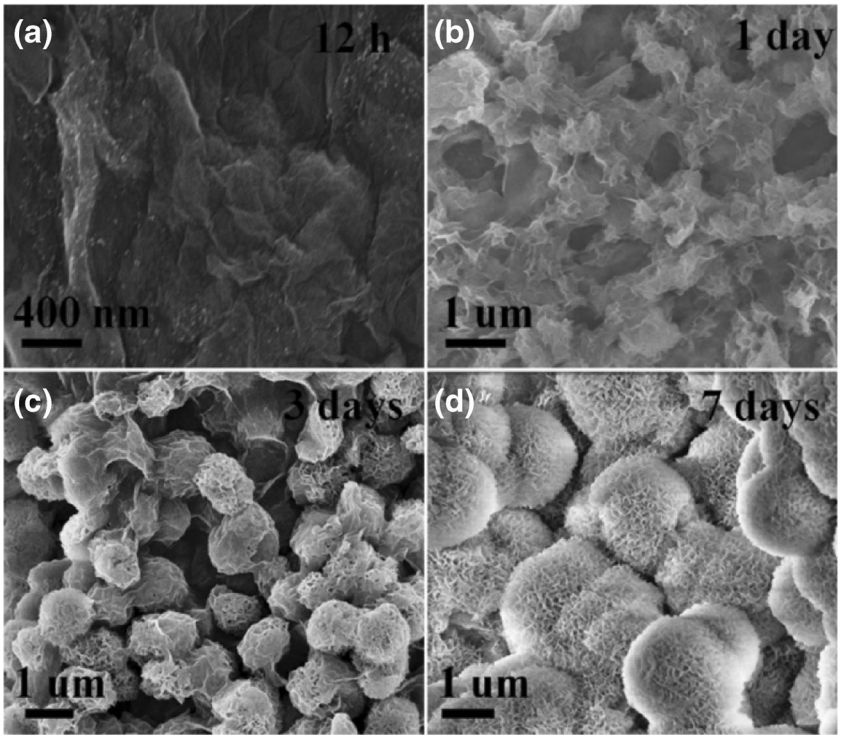

Fig. 4 The process of HAp nucleation and growth on GO. SEM images of the GO after **a** 12 h, **b** 1 day, **c** 3 days, and **d** 7 days of immersion in a 1.5 × simulated body fluid aqueous solution. Reprinted with permission from Royal Society of Chemistry [69]

amino groups in PANI units enhanced the coordinate ability of sulfonic groups on LS chains and carboxyl groups on GO nanosheets for Pb(II). An optimal adsorption pH of 5.0 was observed for the LS-GO-PANI, and 98.3% of its maximum adsorption capacity could be reached in 4 h. Pb(II) concentrations and LS-GO-PANI amounts had an effect on the adsorption capacity and adsorptivity, which could further utilized to enhance the adsorption of Pb(II).

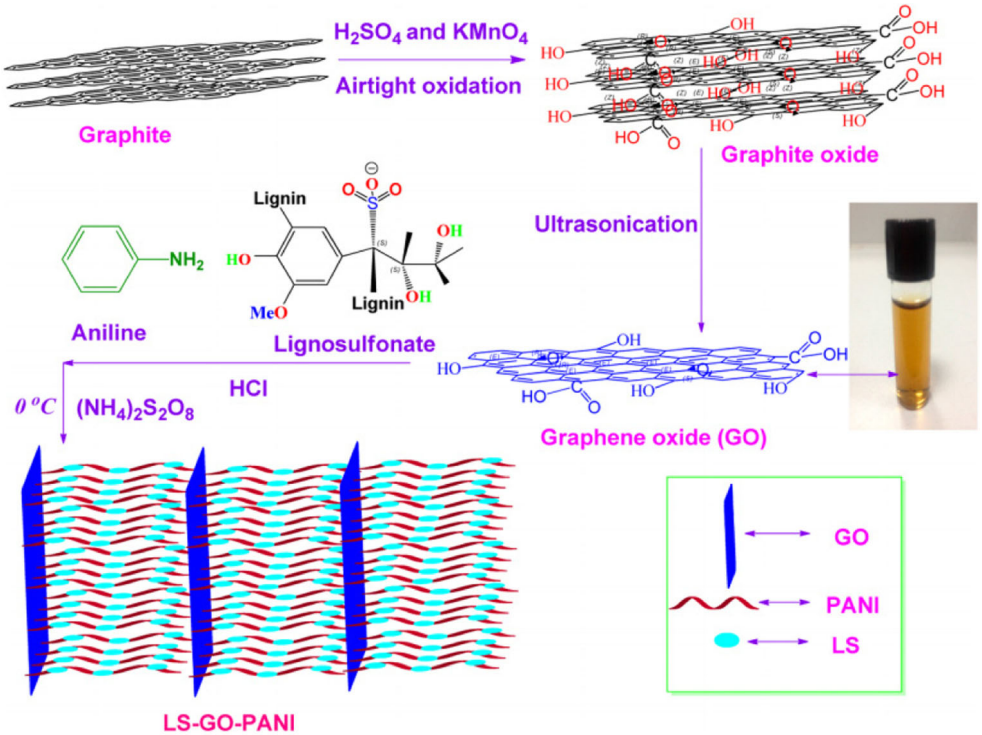

Fig. 5 Preparation process of LS-GO-PANI ternary nanocomposites. Reprinted with permission from American Chemical Society [70]

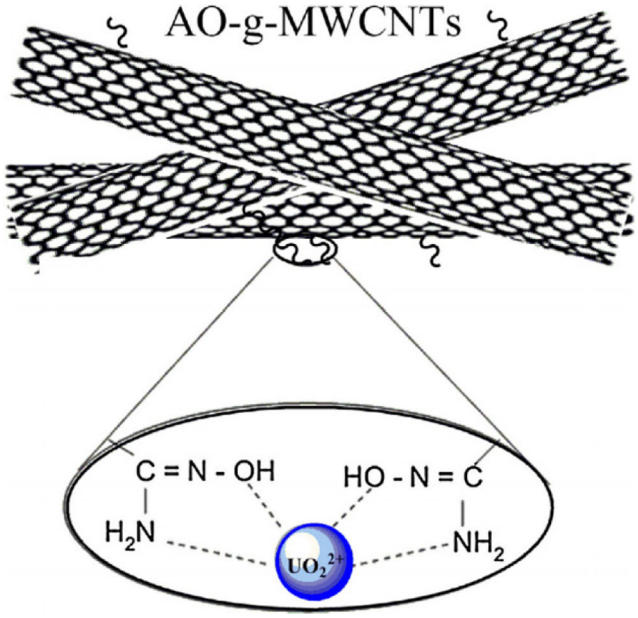

Fig. 6 Probable mechanism for adsorption of U(VI) by AO-g-MWCNTs. Reprinted with permission from Elsevier [86]

2.2 Carbon nanotube-based nanoadsorbents

Carbon nanotubes (CNTs) are allotropes of carbon that are long, thin, and cylindrical, about 1–3 nm in diameter and hundreds to thousands of nanometers long. They are a kind of graphite material and can be viewed as rolled up graphene sheets [71, 72]. CNTs are mainly divided into single-walled CNTs (SWCNTs) and multiwalled CNTs (MWCNTs) [73, 74]. SWCNTs have only a single layer of graphene, while MWCNTs are made up of multiple rolled layers of graphene. CNTs can be treated by acid, such as nitric acid and sulfuric acid, and potassium permanganate, to form oxidized CNTs [75–78]. Compared to CNTs, oxidized CNTs become polar and easy to disperse in water. CNTs and graphene are quite similar in many aspects, like their compositions, electrical, thermal, and optical properties [79]. Therefore, CNTs can be applied to such areas as electronics, energy, and sensors [80–83]. They are also an effective adsorbent for metal ion removal from water [84, 85].

Wang et al. [86] prepared amidoxime-grafted MWCNTs (AO-g-MWCNTs) to adsorb U(VI) from nuclear industrial effluents. Oxidized MWCNTs were first treated by N_2 plasma and then grafted with acrylonitrile (AN) to produce AN-g-MWCNTs. The cyano groups on the AN-g-MWCNTs were converted to amidoxime groups by a reaction with the hydroxylamine hydrochloride. Compared to oxidized MWCNTs, AO-g-MWCNTs had a rougher surface and more compact stacking morphology. N_2 adsorption-desorption experiments showed that the BET-specific surface area of oxidized MWCNTs decreased from 91.31 to 72.59 m^2/g after plasma grafting. The adsorption behaviors of U(VI) onto AO-g-MWCNTs were systematically investigated. As the initial pH of the U(VI) solution increased from 1 to 4.5, the distribution coefficient of U(VI) gradually became larger. It only needed about 1 h to reach the adsorption equilibrium, and the adsorption kinetics could be best described by the pseudo-second-order model ($R^2 = 0.9997$). The Langmuir isotherm model revealed that AO-g-MWCNTs had a much higher maximum adsorption capacity than oxidized MWCNTs, which meant that AO could significantly enhance the adsorption ability of MWCNTs. Temperature also affected the adsorption of U(VI), and higher temperatures were favorable. The thermodynamic studies indicated that the adsorption process was spontaneous and U(VI) was more likely to be adsorbed by AO-g-MWCNTs than by oxidized MWCNTs. AO-g-MWCNTs exhibited much higher selectivity towards U(VI) over other coexisting metal ions, such as Ni(II), Zn(II), Cs(I), and Ba(II), and showed great removal performance for U(VI) from seawater. The adsorption mechanism of AO-g-MWCNTs was believed to be that U(VI) combined

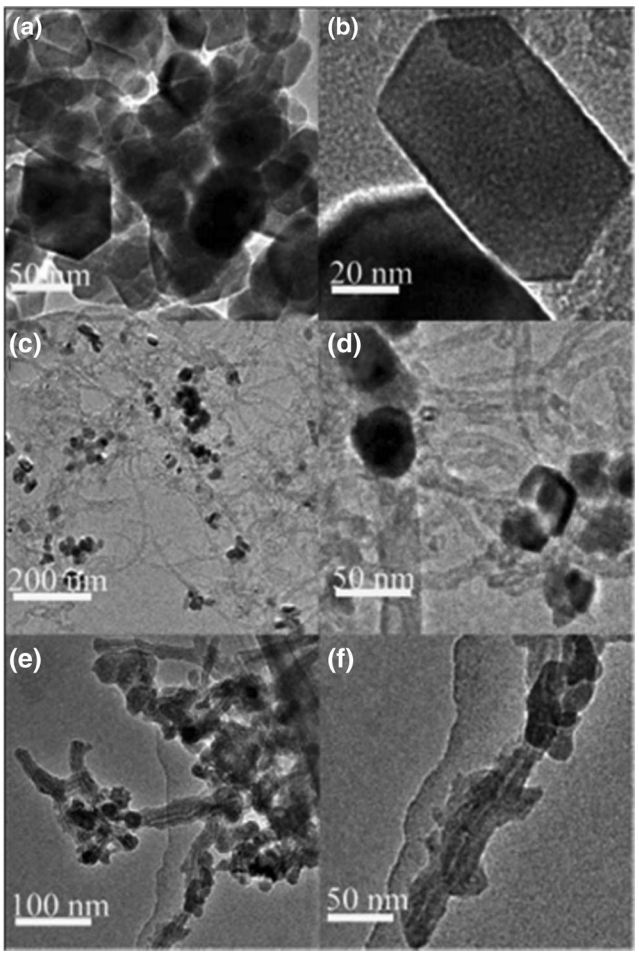

Fig. 7 TEM images of **a**, **b** pure Fe_3O_4 nanoparticles, **c**, **d** Fe_3O_4/o-MWCNTs nanocomposites, and **e**, **f** PmPD/Fe_3O_4/o-MWCNTs nanocomposites at different magnifications. Reprinted with permission from Royal Society of Chemistry [87]

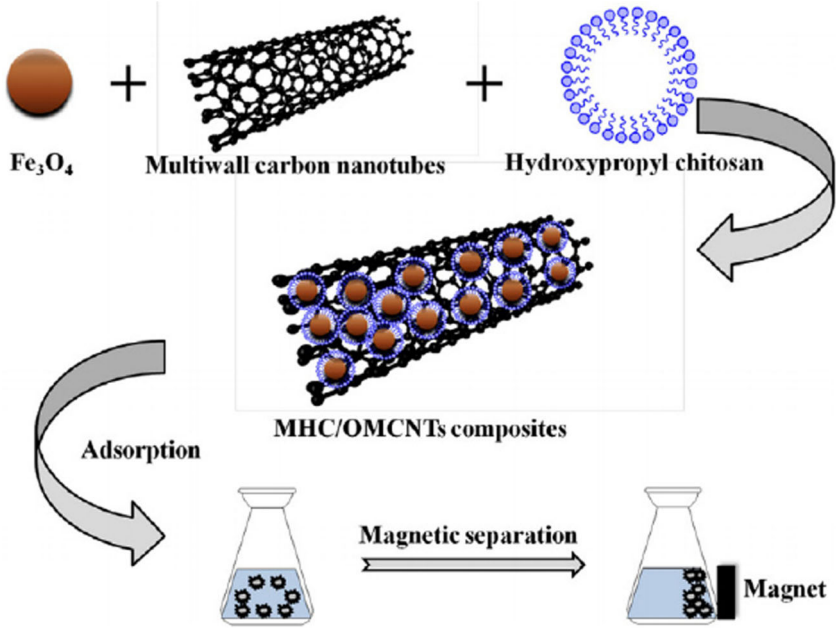

Fig. 8 Preparation of MHC/o-MWCNT composites and their application for Pb(II) removal. Reprinted with permission from Elsevier [88]

oxygen and nitrogen atoms of amidoxime groups to form complexes to achieve the removal of U(VI), as shown in Fig. 6. The AO functionalized MWCNTs, as a quite effective adsorbent, showed great potential applications in practice.

Tian et al. [87] synthesized poly(m-phenylenediamine)-coated iron oxide/acid-oxidized MWCNTs (PmPD/Fe_3O_4/o-MWCNTs) magnetic nanocomposites via in situ oxidative polymerization for Cr(VI) removal for the first time. The morphology of the nanocomposites at different stages in the synthesis process was shown in Fig. 7. BET calculation revealed that Fe_3O_4/o-MWCNTs and PmPD/Fe_3O_4/o-MWCNTs had a much lower pore volume, specific surface area, and pore size

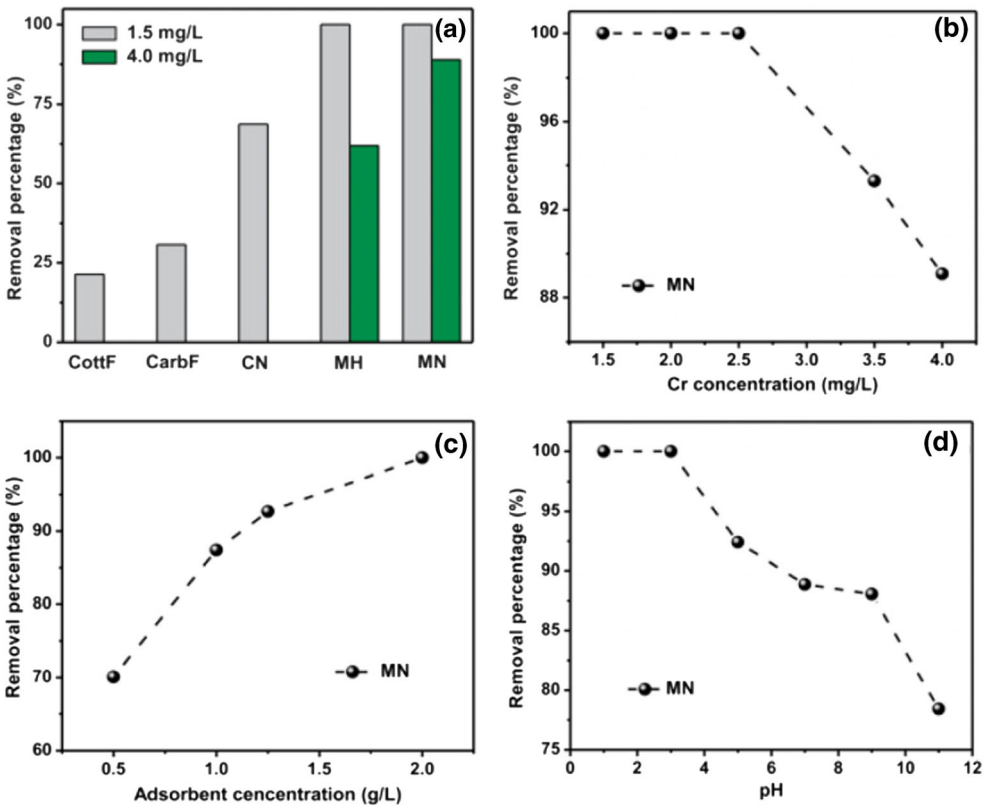

Fig. 9 **a** The Cr(VI) removal performance of different materials (adsorbent 1.0 g/L; treating time 10 min; pH 7); **b** effect of the initial Cr(VI) concentration on the Cr(VI) removal performance (MN 1.0 g/L; treating time 10 min; pH 7); **c** Cr(VI) removal percentage at different MN concentrations (initial Cr(VI) concentration 4.0 mg/L; treating time 10 min; pH 7); **d** effect of the solution pH on the Cr(VI) removal efficiency (MN 1.0 g/L; initial Cr(VI) concentration 4.0 mg/L; treating time 10 min). Reprinted with permission from Royal Society of Chemistry [93]

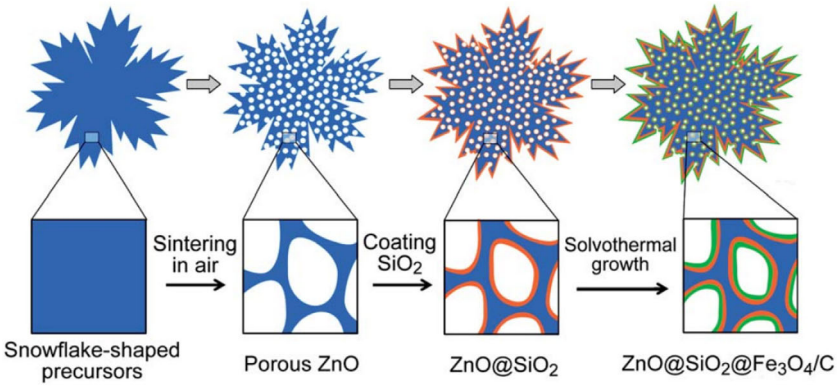

Fig. 10 Preparation process of snowflake-shaped magnetic ZnO@SiO_2@Fe_3O_4/C micro −/nanostructures. Reprinted with permission from the Royal Society of Chemistry [94]

than o-MWCNTs, and the reason was believed to be that Fe_3O_4 nanoparticles and PmPD blocked the pore entrances on the o-MWCNTs. The adsorption capacities of PmPD/Fe_3O_4/o-MWCNTs, raw-MWCNTs, o-MWCNTs, and Fe_3O_4/o-MWCNTs were in the order of PmPD/Fe_3O_4/o-MWCNTs > Fe_3O_4/o-MWCNTs > o-MWCNTs > raw-MWCNTs. Effects of the initial pH of the solution on the adsorption of Cr(VI) onto PmPD/Fe_3O_4/o-MWCNTs were investigated, and the results showed that the adsorption capacity decreased as the pH increased from 2 to 11. Langmuir, Freundlich, and Temkin isotherm models were respectively used to describe the adsorption behaviors of Cr(VI), and the Langmuir model fitted the adsorption data best. As the temperature increased from 273 to 333 K, the maximum adsorption capacity calculated from the Langmuir model increased from 219.8 to 346.0 mg/g. Adsorption dynamic studies showed that both the pseudo-first-order model and pseudo-second-order model could be employed to simulate the adsorption kinetics, and the pseudo-second-order equation gave a relatively higher correlation coefficient (R^2 > 0.99). Thermodynamic studies indicated that the adsorption of Cr(VI) onto PmPD/Fe_3O_4/o-MWCNTs was a spontaneous and endothermic process. After adsorption, PmPD/Fe_3O_4/o-MWCNTs could be easily separated through an external magnetic field, and its adsorption capacity decreased by less than 48% after five consecutive recycles. Both PmPD groups and Fe_3O_4 particles played an important role in the adsorption of Cr(VI), and the adsorption mechanism included physical and chemical adsorptions. In conclusion, PmPD/Fe_3O_4/o-MWCNT was a good candidate for wastewater treatment.

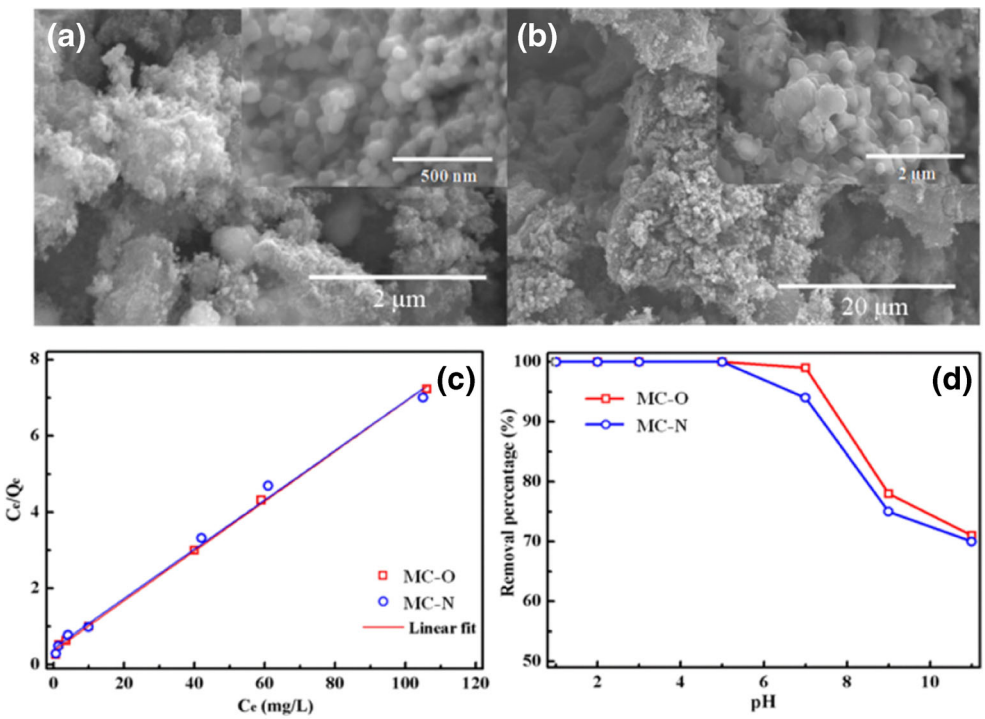

Fig. 11 SEM images of **a** MC-O and **b** MC-N; **c** Cr(VI) adsorption isotherm fitted by Langmuir model (adsorbent dosage 50.0 mg; volume 20.0 mL; initial Cr(VI) concentration 1.0–10.0 mg/L; treating time 30 min; pH 7); **d** effect of the solution pH on the Cr(VI) removal performance (adsorbent dosage 50.0 mg; volume 20.0 mL; initial Cr(VI) concentration 4.0 mg/L; treating time 10 min). Reprinted with permission from the Royal Society of Chemistry [95]

Table 2 Adsorption capacity comparison of different carbon nanoadsorbents

Adsorbent	Metal ions	pH	T (K)	Maximum adsorption capacity (mg/g)[a]	Ref.
Sulfuric acid-doped poly diaminopyridine/graphene composite (G-PDAP)	Cr(VI)	1	Room temperature	609.76	[99]
Graphene manganese ferrite ($MnFe_2O_4$-G) composite	Pb(II), Cd(II)	5 for Pb, 7 for Cd	310	100 for Pb, 76.9 for Cd	[100]
Fe_3O_4 nanoparticles hybridized with graphene (Fe_3O_4/G)	Cr(VI)	–	–	78.5	[101]
Magnetically recoverable graphene/Fe_3O_4 composite (GFC)	Zn(II), Ni(II)	7	303	121.5 for Zn, 111.4 for Ni	[102]
Magnetic cobalt and nickel ferrites with graphene nanocomposites ($CoFe_2O_4$-G, $NiFe_2O_4$-G)	Pb(II), Cd(II)	5 for Pb(II), 7 for Cd(II)	310	142.85 for Pb(II) by $CoFe_2O_4$-G; 111.11 for Pb(II) by $NiFe_2O_4$-G; 105.26 for Cd(II) by $CoFe_2O_4$-G; 74.62 for Cd(II) by $NiFe_2O_4$-G	[103]
Polyacrylamide-grafted graphene (PAM-g-graphene)	Pb(II)	6	293	819.67	[67]
$CoFe_2O_4$-chitosan-graphene (MCGS)	Hg(II)	7	323	361	[104]
Amino-functionalized magnetic graphene composite (Fe_3O_4-GS)	Cr(VI), Pb(II), Cd(II), Hg(II), Ni(II)	–	Room temperature	39.92 for Cr, 157.9 for Pb, 163.6 for Cd, 167.8 for Hg, 158.5 for Ni	[105]
CdS/graphene nanocomposite, ZnS/graphene nanocomposite	Pb(II), Cd(II)	5.9	Room temperature	3.10 for Pb by CdS/graphene nanocomposite, 3.62 for Cd by ZnS/graphene nanocomposite	[106]
Graphene-Fe_3O_4 (G-Fe_3O_4) nanocomposite	Pb(II)	5	310	69	[107]
Nanoscale zero-valent iron particles supported on rGO (NZVI/rGOs)	Cd(II)	5	293	425.72	[108]
Nanoscale zero-valent iron particles supported on rGO (NZVI/rGOs)	Pb(II), Cr(VI)	5	293	396.37 for Pb, 187.16 for Cr	[109]
rGO/Fe_3O_4 (GF) composites	Cr(VI)	2	room temperature	14.95	[110]
α-MnO_2 nanosheets integrated on NH_2 graphene (α-MnO_2-NH_2-rGO)	Cr(VI)	2	328	371	[111]
Poly(o-phenylenediamine)/rGO (PoPD/rGO) composite nanosheets	Pb(II)	–	room temperature	228	[112]
Magnetic cobalt ferrite-rGO nanocomposites ($CoFe_2O_4$-rGO)	Pb(II), Hg(II)	5.3 for Pb, 4.6 for Hg	298	299.4 for Pb, 157.9 for Hg	[113]
Magnetite-GO (mGO) hybrid	Sr(II), Co(II)	7	338	22.3 for Sr, 28.5 for Co	[114]
Polydopamine/GO (PD/GO) composites	U(VI)	4.0	293	145.39	[115]
Ag-$CoFe_2O_4$-GO nanocomposite	Pb(II)	7	310	63.596	[116]
L-Tryptophan functionalized GO (GO/L-Trp)	Cu(II), Pb(II)	5 for Cu, 4 for Pb	293	588 for Cu(II), 222 for Pb(II)	[117]
Magnetite-GO-layered double-hydroxide (MGL) composites	Pb(II)	5	298	173	[118]
Poly(allylamine hydrochloride)-functionalized GO nanosheets (PAH-GO composite)	Cu(II)	6	293	396.83	[119]
Diethylenetriamine-functionalized magnetic GO nanocomposite (GO-Fe_3O_4-DETA)	Pb(II), Cd(II)	5.5	–	172.41 for Pb, 59.88 for Cd(II)	[55]
Ammonia-modified GO (NH_3-GO)	U(VI)	6	298	80.13	[120]
Manganese dioxide/iron oxide/GO magnetic nanocomposites (MnO_2/Fe_3O_4/GO)	Cr(VI)	2	298	193.1	[121]
Chitosan/GO nanofibers	Pb(II), Cu(II), Cr(VI)	6 for Pb and Cu, 3 for Cr	318	461.3 for Pb, 423.8 for Cu, 310.2 for Cr	[122]

Table 2 (continued)

Adsorbent	Metal ions	pH	T (K)	Maximum adsorption capacity (mg/g)[a]	Ref.
Magnetic carbonate hydroxyapatite/GO (M-CHAP/GO)	Pb(II)	4.5	308	271.7	[123]
L-cystine functionalized exfoliated GO (EGO)	Hg(II)	5.5–7	–	79.36	[68]
Polyethylenimine-modified magnetic GO (GO/Fe_3O_4/PEI) nanocomposites	Cu(II)	5	298	157.48	[124]
Poly(sodium acrylate)-GO (PSA-GO) double network hydrogel	Cd(II), Mn(II)	6	303	238.3 for Cd, 165.5 for Mn	[125]
GO-cadmium sulfide composite with addition of ethylenediamine (GO/CdS(en))	Cu(II)	6	298	137.174	[126]
Aminosilanized GO nanosheets (GO-NH_2)	Pb(II)	6	298	96	[127]
GO-$MnFe_2O_4$ magnetic nanohybrids (GONH)	Pb(II), As(III), As(V)	5 for Pb, 6.5 for As(III), 4 for As(V)	–	673 for Pb, 146 for As(III), 207 for As(V)	[128]
Few-layered GOs (GOs)	Pb(II)	5.8	333	747.99	[129]
Three-dimensional magnetic GO foam/Fe_3O_4 nanocomposite (GOF/Fe_3O_4)	Cr(VI)	2	room temperature	258.6	[130]
Lignosulfonate-GO-polyaniline (LS-GO-PANI) nanocomposite	Pb(II)	5	303	250	[70]
Amination GO (GO-NH_2) nanosheets	Co(II)	6	298	116.35	[131]
Fe_3O_4/SiO_2-decorated GO nanocomposites (Fe_3O_4/SiO_2-GO)	Cr(III)	5.8	298	4.7	[132]
Polyethyleneimine-modified GO (PEI-GO)	Cr(VI)	2	298	581	[133]
GO-hydroxyapatite (GO-HAp) nanocomposites	Sr(II)	7	298	702.18	[69]
Magnetic prussian blue/GO (PB/Fe_3O_4/GO) nanocomposites	Cs(I)	7	298	55.56	[134]
EDTA-functionalized magnetic GO (GO-Fe_3O_4-EDTA)	Pb(II), Hg(II), Cu(II)	4.2 for Pb(II), 4.1 for Hg(II), 5.1 for Cu(II)	318	508.4 for Pb(II), 268.4 for Hg(II), 301.2 for Cu(II)	[135]
Dithiocarbamate groups functionalized MWCNTs (DTC-MWCNTs)	Cd(II), Cu(II), Zn(II)	6 for Cd and Zn, 5 for Cu	298	202.429 for Cd, 101.523 for Cu, 16.625 for Zn	[136]
Cobalt ferrite/MWCNTs ($CoFe_2O_4$/MWCNTs) magnetic hybrids	U(VI)	6	298	212.7	[137]
CNT-polydopamine-polyethylenimine (CNT-PDA-PEI)	Cu(II)	7	298	70.9	[138]
Amidoxime-grafted MWCNTs (AO-g-MWCNTs)	U(VI)	4.5	298	176	[86]
Magnetic MWCNT/iron oxide composite (Fe_3O_4/MWCNT)	U(VI)	5.5	343	27.61	[139]
Carboxylated MWCNT-Fe_3O_4 magnetic hybrids (c-MWCNTMCs)	Cu(II)	6	298	60.6	[140]
Chitosan-functionalized MWCNTs coated with magnetic amino-modified $CoFe_2O_4$ nanoparticles (MNP-CTS)	Pb(II)	6	–	140.4	[141]
Activated alumina-CNT nanoclusters	Cr(VI), Cd(II)	2 for Cr, 7.5 for Cd	303	264.5 for Cr, 229.9 for Cd	[142]
Magnetic hydroxypropyl chitosan/oxidized MWCNTs (MHC/o-MWCNTs) composites	Pb(II)	5	298	116.3	[88]
Tartaric acid-modified MWCNTs (MWCNT-TA)	Cu(II)	6	298	30.85	[143]
Oxidized MWCNTs (o-MWCNTs)	Pb(II), Cu(II), Cr(VI), Cd(II), Ni(II)	5.5	298	75 for Pb, 70.4 for Cu, 67 for Cr, 66 for Cd, 59.2 for Ni	[144]
Oxidized MWCNTs (o-MWCNTs)	Cd(II)	5	323	83.33	[145]
Oxidized MWCNTs (o-MWCNTs)	V(V)	5	298	100	[146]
Oxidized MWCNTs (o-MWCNTs)	Cr(VI)	–	323	2.517	[147]
Oxidized MWCNTs (o-MWCNTs)	Au(III)	2	298	62.5	[76]

Table 2 (continued)

Adsorbent	Metal ions	pH	T (K)	Maximum adsorption capacity (mg/g)[a]	Ref.
Poly(m-phenylenediamine)-doped iron oxide/acid-oxidized MWCNTs nanocomposite (PmPD/Fe_3O_4/o-MWCNTs)	Cr(VI)	2	333	346	[87]
Hydroxyapatite-coated granular-activated carbon (C-HAp) nanocomposite	Pb(II)	6	298	9.31	[148]
Magnetite-powder-activated carbon (M-PAC)	Ni(II), Co(II), Cd(II)	6	293	56.026 for Ni, 58.23 for Co, 63.52 for Cd	[149]
Carbon nanofibers grown on powdered-activated carbon (PAC-CNFs)	Pb(II)	5.5	301	166.66	[98]
[C/Fe_3O_4]@C coaxial nanocables	Cu(II)	6	298	64.0615	[96]
Fe_3O_4@C@MgAl-layered double-hydroxide (LDH) nanoparticles	Cr(VI)	6	313	192.307	[150]
Magnetic porous γ-Fe_2O_3/C@HKUST-1 composites	Cr(VI)	3	303	105	[151]
Snowflake-shaped ZnO@SiO_2@Fe_3O_4/C micro−/nanostructures	Pb(II), As(V)	7	298	94.3 for Pb, 23.6 for As	[94]
Hybrid γ-Fe_2O_3/carbon hollow spheres	Pb(II), Cr(VI)	–	Ambient temperature	614 for Pb, 449 for Cr	[97]

[a] The maximum adsorption capacity is calculated based on Langmuir adsorption isotherm model

Magnetic hydroxypropyl chitosan/oxidized MWCNT (MHC/o-MWCNT) composites were successfully fabricated and employed as the adsorbent for Pb(II) removal from an aqueous solution, as shown in Fig. 8 [88]. Magnetic Fe_3O_4 nanoparticles were first prepared from $FeCl_3 \cdot 6H_2O$, and then MWCNTs were oxidized by a mixture of concentrated sulfuric acid and nitric acid to produce o-MWCNTs. Afterwards, magnetic Fe_3O_4 nanoparticles and o-MWCNTs were sequentially added to the hydroxypropyl chitosan solution, and MHC/o-MWCNTs composites were assembled. The MHC/o-MWCNTs composites showed an impressive adsorption performance with an adsorption capacity of 116.3 mg/g. Moreover, they exhibited a rapid response to the external magnetic field, and the separation time was as fast as 3 min after adsorption. Sips isotherm model was found more suitable than Langmuir, Freundlich, and Dubinin-Radushkevich isotherm models to describe the adsorption behaviors of Pb(II) onto MHC/o-MWCNTs composites. The thermodynamic parameters, such as free energy − 2.304 KJ/mol, enthalpy 39.03 KJ/mol, and entropy 138.7 J/(mol·K), illustrated that the adsorption process was endothermic and spontaneous. The MHC/o-MWCNTs composites were an ideal adsorbent to remove Pb(II) from water.

2.3 Other carbon-based nanoadsorbents

Graphene and CNTs are the two most widely studied carbon nanoadsorbents. Besides them, there are many other carbon nanomaterials that are used as nanoadsorbents, such as carbon nanofabrics, nanofibers, nanocables, and nanofloral clusters. These carbon nanoadsorbents often exhibit some distinctive characteristics due to their different architectures, which may bring about outstanding adsorption performance, economical costs, and easy recovery [89–92].

Zhu et al. [93] employed conventional and microwave-assisted annealing methods, respectively, to synthesize mesoporous magnetic carbon fabric nanocomposites for Cr(VI) removal. For comparison, Fig. 9a shows the removal percentage of different adsorbents in neutral solution. Both MH and MN (magnetic carbon fabric nanocomposites prepared by microwave annealing in a 5% H_2-Ar and N_2 atmosphere, respectively) exhibited complete Cr(VI) removal at an initial Cr(VI) concentration of 1.5 mg/L, while CN (magnetic carbon fabric nanocomposites fabricated via conventional annealing under a N_2 atmosphere) only had 68.7% of Cr(VI) removed, and even lower values were reported for cotton fabrics (CottF, 21.3%) and carbon fabrics (CarbF, 30.7%). The MN had a higher removal percentage than MH when the initial concentration of Cr(VI) was 4.0 mg/L. Figure 9b illustrated the effect of initial Cr(VI) concentration on the removal efficiency of MN. A maximum removal percentage of 100% was achieved for the initial Cr(VI) concentration of 1.5, 2.0, and 2.5 mg/L. However, the removal percentage decreased with Cr(VI)

Table 3 Adsorption isotherm models

Model	Equation	Ref.
Langmuir	$Q_e = \frac{Q_m K_L C_e}{1+K_L C_e}$	[139, 143]
Freundlich	$Q_e = K_F C_e^{1/n}$	[136, 138]
Dubinin-Radushkevich	$Q_e = Q_m e^{-k\varepsilon^2}$	[111, 164]
Temkin	$Q_e = \frac{RT}{b}\ln K_T + \frac{RT}{b}\ln C_e$	[87, 120]
Redlich-Peterson	$Q_e = \frac{K_R C_e}{1+\alpha_R C_e^{\beta}}$	[102, 122]
Sips	$Q_e = \frac{Q_m \alpha_s C_e^{1/n}}{1+\alpha_s C_e^{1/n}}$	[88, 125]
Henry	$Q_e = K_H C_e$	[105, 135]

concentration further increasing. Figure 9c indicates the Cr(VI) removal performance at different MN concentrations. The removal percentage increased with the increase of MN loadings. The maximum removal percentage of 100% could be achieved with an MN loading of 2.0 g/L. The pH effect on the removal efficiency of Cr(VI) using MN was revealed in Fig. 9d. The MN showed stronger removal ability when the pH was lower than 3. With an increasing pH value, the removal percentage decreased (about 78.4% at pH 11). The MN had an adsorption capacity of 3.74 mg/g, which was much higher than carbon-coated magnetic nanoparticles (1.52 mg/g) and graphene nanocomposites (1.03 mg/g).

Conventional micro−/nanostructured adsorbents often suffer from unfavorable aggregation, which will lead to overlap and coverage of numerous adsorption sites. As a result, their adsorption efficiency seriously decreased. A snowflake-shaped magnetic ZnO@SiO_2@Fe_3O_4/C micro−/nanostructure was prepared, as shown in Fig. 10 [94]. First, a snowflake-shaped porous ZnO micro−/nanostructure was fabricated through a facile hydrothermal route followed by a sintering process. Then, the ZnO micro−/nanostructures were coated with SiO_2 layers via the Stöber method. Next, magnetic Fe_3O_4/C composite coatings were grown onto the ZnO@SiO_2 micro−/nanostructures through a solvothermal approach. The prepared ZnO@SiO_2@Fe_3O_4/C micro−/nanostructures could keep a relatively large space between themselves, which significantly reduced the aggregation of micro−/nanostructures and the overlap of adsorption sites. Compared with magnetic ZnO@SiO_2@Fe_3O_4/C microspheres prepared by the similar procedures, the snowflake-shaped magnetic ZnO@SiO_2@Fe_3O_4/C micro−/nanostructures exhibited a much higher adsorption efficiency. The maximum adsorption capacities for Pb(II) and As(V) were 94.3 and 23.6 mg/g, respectively, while for the magnetic ZnO@SiO_2@Fe_3O_4/C microspheres, those were only 54.6 and 17.2 mg/g. The mechanism for the enhancement was demonstrated from the special biomimetic structure.

Table 4 Adsorption kinetic models

Model	Equation	Ref.
Pseudo-first-order	$Q_t = Q_e\left(1-e^{-k_1 t}\right)$	[75, 165]
Pseudo-second-order	$Q_t = \frac{k_2 Q_e^2 t}{1+k_2 Q_e t}$	[104, 166]
Intraparticle diffusion	$Q_t = k_{di} t^{1/2} + C$	[167, 168]
Elovich	$Q_t = \frac{1}{\beta}\ln(\alpha\beta) + \frac{1}{\beta}\ln t$	[169, 170]
Bangham	$\ln Q_t = \ln k_b + \frac{1}{m}\ln t$	[123]

Magnetic carbon-iron nanoadsorbents fabricated by carbonizing cellulose and reducing Fe_3O_4 nanoparticles or $Fe(NO_3)_3$ (denoted as MC-O and MC-N, respectively) had demonstrated great Cr(VI) removal ability [95]. The SEM images (Fig. 11 a, b) showed that they presented spherical particles with an average diameter of ~ 100 and 250 nm for MC-O and MC-N, respectively. A higher portion of zero-valence iron (ZVI) and a larger specific surface area were observed for the MC-N than the MC-O. Both MC-O and MC-N exhibited a great Cr(VI) removal performance. For example, 4.0 mg/L Cr(VI) neutral solution could be purified by 2.5 g/L MC-O and MC-N within 10 min, and 1000 mg/L Cr(VI) could be completely removed from the solution in 10 min at pH 1.0. The equilibrium adsorption data could be well fitted for Langmuir isotherm model (Fig. 11c). Meanwhile, the Cr(VI) removal by both MC-O and MC-N was highly pH dependant (Fig. 11d), and the removal percentage decreased with the pH value increasing in solutions. MC-N and MC-O revealed removal capacities of 327.5 and 293.8 mg/g at pH 1.0, respectively, which were much higher than many other adsorbents, such as magnetic chitosan (55.8 mg/g), magnetic carbon fabricated by rice husk (30.96 mg/g), and polypyrrole-polyaniline nanofibers (227.22 mg/g). For the removal mechanisms, it was believed that Cr(VI) was first reduced to Cr(III) by the ZVI, and then the Cr(III) was removed from the solution through precipitation and adsorption.

Han et al. [96] successfully fabricated [C/Fe_3O_4]@C electricity-magnetism-adsorption trifunctional coaxial nanocables by carbonization of the electrospun [polyacrylonitrile/ferric acetylacetonate]@polyacrylonitrile coaxial nanocables. The as-prepared [C/Fe_3O_4]@C coaxial nanocables had obvious core-shell structure with a core diameter of 125 nm and shell thickness of 82 nm. Magnetic Fe_3O_4 nanoparticles were scattered in core of carbon matrix and displayed a positive effect on electrical conductivity. Efficient adsorption of Cu(II) from an aqueous solution was observed using [C/Fe_3O_4]@C coaxial nanocables as the adsorbent. Cui et al. [97] synthesized hybrid

γ-Fe_2O_3/carbon hollow nanospheres with a predominant orientation (1 1 1) plane of γ-Fe_2O_3 and rich oxygen-containing functional groups on carbon via a one-step hydrothermal method. The hybrid γ-Fe_2O_3/carbon hollow nanospheres exhibited high adsorption capacities and rapid removal abilities for Pb(II) and Cr(VI). They could be easily recovered through an external magnetic field after adsorption. Mamun et al. [98] prepared carbon nanofibers (CNFs) by chemical vapor deposition method in which C_2H_2 was employed as carbon source and Ni(II) catalyst impregnated oil palm kernel shell-based powdered-activated carbon (PAC) was used as fixed substrate for the growth of CNFs. The PAC-CNFs porous nanocomposites were found to be good for adsorption of Pb(II). The adsorption kinetics and isotherm were carefully investigated, and all the results showed that the PAC-CNFs porous nanocomposites had potential for Pb(II) removal from an aqueous solution.

2.4 Comparison

Table 2 summarizes the adsorption data of some modified carbon nanomaterials that were recently reported. Their maximum adsorption capacities are compared, and the corresponding adsorbed metal ions are illustrated.

It can be seen from Table 2 that graphene and CNTs are the two most often used carbon nanoadsorbents. In fact, most modified carbon nanoadsorbents involve graphene and CNTs composites. Besides that, polymers, especially those with electron-donating or alkaline groups, are increasingly applied to various carbon nanoadsorbents. They have many advantages over other materials, such as tailored molecular weight, chain topology, and functional groups [152–154]. Moreover, they are usually nontoxic as a result of their large molecular size, which will dramatically reduce the secondary pollution [155, 156]. The plentiful active groups of polymers can significantly enhance the adsorption performance, and more possible ways are provided to achieve the desorption and recovery of adsorbents in an easy manner with the advent of stimuli-responsive polymers [157–159]. In a word, it becomes more and more popular utilizing polymers to modify carbon nanoadsorbents.

3 Analysis and discussion

Based on the above summary, some common modification methods, various adsorption isotherm and kinetic models, and diverse adsorption mechanisms can be concluded.

3.1 Modification methods

The removal process of metal ions from wastewater mainly includes three steps: adsorption, desorption, and recovery. Carbon nanomaterials are always modified to optimize their performances in these areas by changing their morphologies or molecular structures. Some commonly used modification methods can be found by analyzing papers broken into the categories of magnetic carbon nanomaterials, electron-donating group grafted-carbon nanomaterials, mixed or filled carbon nanomaterials, and carbon nanomaterials with modified morphologies.

3.1.1 Magnetic carbon nanomaterials

Adsorbents should ideally be well-dispersed in water during the adsorption process and be easy to aggregate during the recovery process. However, it seems there are contradictions between these two processes because usually the better the dispersion of an adsorbent is, the more difficult the separation of it will be. Adsorbent particles with a smaller size are often easier to form a uniform solution than those with a larger size, but they are usually harder to be separated by such methods as filtration, centrifugation, and gravity sedimentation. Magnetic separation is an effective way to solve the above problem. It is a physical, easy to operate, economical, and environmentally friendly process. The adsorbents can be easily separated by applying an external magnetic field after introducing some magnetic materials into them. These magnetic materials often not only facilitate the recovery of adsorbents but also improve their adsorption ability. For graphene-based nanoadsorbents, they can even inhibit the aggregation of graphene nanosheets. Some frequently used magnetic materials are Fe_3O_4, γ-Fe_2O_3, and MFe_2O_4 (M = Zn, Mg, Co, Cu, Ni, Mn, etc.) [100, 101, 103, 104, 151].

Tan et al. [137] synthesized cobalt ferrite/MWCNTs ($CoFe_2O_4$/MWCNTs) magnetic hybrids by a hydrothermal method. The surface area and pore volume of $CoFe_2O_4$/MWCNTs were much larger than those of $CoFe_2O_4$. Compared to MWCNTs and $CoFe_2O_4$, $CoFe_2O_4$/MWCNTs showed a far higher adsorption capacity for U(VI). U(VI)-loaded $CoFe_2O_4$/MWCNTs could be easily separated from the solution by using a magnet. Chella et al. [100] fabricated graphene manganese ferrite ($MnFe_2O_4$-G) nanocomposite through a modified Hummer's method and solvothermal process for the removal of Pb(II) and Cd(II). The existence of $MnFe_2O_4$ nanoparticles not only improved the adsorption capacity of graphene but also enhanced its antibacterial activity. Fe_3O_4 nanoparticles with an average size of 17 nm were successfully synthesized and decorated onto the surface of GO via ultrasound-assisted precipitations [114]. The as-prepared GO-Fe_3O_4 hybrid exhibited high adsorption efficiency for Co(II) and Sr(II), especially for Co(II) arisen from its close similarity to Fe(II) in the magnetite.

3.1.2 Electron-donating group grafted carbon nanomaterials

Since metal ions are positively charged, an effective method to enhance the adsorption ability of carbon nanomaterials is

grafting electron-donating groups onto them, such as nitrogen, oxygen, sulfur, or chlorine-containing groups. These electron-donating groups can be viewed as bases and metal ions belong to acids based on Lewis acid-base theory. Their interactions include electrostatic interaction, ion exchange, complex formation, and redox reaction [160, 161]. Using this method not only improves the adsorption rate and capacity but also optimizes the dispersity of carbon nanomaterials in water due to the stronger hydrophilicity of grafted atoms in comparison with carbon atoms. The adsorption selectivity can also be enhanced by introducing some specific groups with high selectivity.

Based on the attraction of N atoms in amine groups to heavy metal ions which arises from their long pair electrons, Tan et al. [117] employed L-tryptophan to aminate GO to investigate its removal performance for Cu(II) and Pb(II). A greatly enhanced adsorption capacity was obtained. After three recycle loops, the L-tryptophan functionalized GO (GO/LTrp) exhibited less than a 5% decrease in adsorption capacity. Li et al. [136] for the first time synthesized dithiocarbamate groups functionalized MWCNT (DTC-MWCNT) to selectively adsorb Cd(II), Cu(II), and Zn(II) from an aqueous solution by reaction of oxidized MWCNTs with ethylenediamine and carbon disulfide. Since Cd(II), Cu(II), and Zn(II) were considered soft acids and dithiocarbamate was a soft base, the DTC-MWCNT exhibited high maximum adsorption capacities. To be more specific, they were 167.2, 98.1, and 11.2 mg/g for Cd(II), Cu(II), and Zn(II), respectively.

3.1.3 Mixed or filled carbon nanomaterials

Each adsorbent has its own characteristics, strengths, and weaknesses. If different adsorbents are added together in a proper way, a new adsorbent will be obtained possessing a performance superior to any individual adsorbent. In addition, dispersing active fillers into the matrix of adsorbents is another quite effective method to enhance their various properties, such as the mechanical strength and chemical stability. These fillers act like the additives in plastics, and some of them include metal oxides, polymers, and biomass. Sui et al. [124] employed polyethylenimine-modified magnetic GO (GO/Fe_3O_4/PEI) nanocomposites to remove Cu(II) from an aqueous solution. Fe_3O_4 nanoparticles first grew on GO sheets, and then the GO/Fe_3O_4 was mixed with PEI to obtain GO/Fe_3O_4/PEI nanocomposites. Superior Cu(II) removal performance was observed, which was attributed to the large surface area of GO, superparamagnetism of Fe_3O_4, and extraordinary complex ability of PEI. The GO and GO/Fe_3O_4/PEI had adsorption capacities of 89.32 and 157.48 mg/g, respectively, which clearly indicated the dominant role of PEI and Fe_3O_4. After 5 cycles of regeneration, the GO/Fe_3O_4/PEI nanocomposites could keep a removal efficiency as high as 84%. Based on the high ion-exchange capability of MgAl-layered double-hydroxide (LDH), strong adsorption ability of mesoporous carbon, and easy recovery of Fe_3O_4 nanoparticles, Zhang et al. [150] designed and developed novel Fe_3O_4@C@MgAl-LDH nanoparticles by chemical self-assembly methods. They could adsorb as much as 152.0 mg/g of Cr(VI) at 40 °C and pH 6.0. Besides the excellent adsorption capacity, they exhibited great reusability, which made them very suitable for the removal of metal ions from wastewater.

3.1.4 Carbon nanomaterials with modified morphologies

Besides to modify the compositions, another way to meet our requirements for some properties of carbon nanoadsorbents is designing and customizing their morphologies. For example, an increase in the surface area and porosity of carbon nanomaterials usually brings about the improvement in the adsorption rate and capacity.

Lei et al. [130] developed a novel three-dimensional (3D) GO foam/Fe_3O_4 nanocomposite (GOF/Fe_3O_4) and evaluated its adsorption performance for Cr(VI). Microwave-plasma chemical vapor deposition techniques were employed to synthesize the free-standing 3D graphene foam on the growth substrate of nickel foam. GOF/Fe_3O_4 was formed after the graphene foam was oxidized and functionalized with Fe_3O_4 nanoparticles through a simple coprecipitation method. The 3D structure provided GOF/Fe_3O_4 with an ultra-high specific surface area of 574.2 m^2/g. Benefiting from that, a maximum adsorption capacity of 258.6 mg/g and equilibrium adsorption rate of 20 min were obtained, which markedly outperformed the performance of reported 2D graphene-based adsorbents and many other conventional adsorbents. Sankararamakrishnan et al. [142] used composite nanofloral clusters of CNTs and activated alumina for removal of Cd(II). CNTs were grown over Fe- and Ni-doped activated alumina by chemical vapor deposition and washed with acid to produce nanofloral clusters. The optimum adsorption condition for Cd(II) was in the pH range of 7–9, and the produced nanofloral clusters had the maximum adsorption capacity of 229.9 mg/g at pH 7.5, which was far higher than that of CNTs, oxidized CNTs, and amino functionalized CNTs. The nanofloral clusters as a promising candidate for wastewater treatment provided new ways to design effective adsorbents.

In practice, many modified carbon nanomaterials have changes in both morphologies and molecular structures. Per actual needs, they are designed and prepared to own some special or enhanced properties. Although there are many ways to enhance the adsorption abilities of carbon nanomaterials, such as changing their sizes, porosities, functional groups, and shapes, most of them aim to increase the contact between adsorbates and adsorption

sites, which is one of the foundations for the development of carbon-based nanoadsorbents.

3.2 Adsorption isotherm, kinetics, and mechanisms

A variety of new modified carbon nanoadsorbents have been developed in the past few years. They may have different structures and properties. However, there are a few common models that can be employed to describe the adsorption of metal ions onto them.

3.2.1 Adsorption isotherm and kinetics

Adsorption isotherm and kinetics are often used to describe the adsorption process, mechanism, and performance. Specifically, adsorption isotherm gives information about adsorption capacities, types of adsorption systems, surface properties of adsorbents, and relationships between adsorbents and adsorbates [162, 163]; information about adsorption rates, rate-limiting steps, and diffusion processes of adsorbates can be given by adsorption kinetics. Tables 3 and 4 listed some usual adsorption isotherm and kinetic models.

Langmuir and Freundlich isotherm models are the two most often used isotherm models. The Langmuir isotherm assumes monolayer adsorption on a homogeneous surface, while the Freundlich isotherm assumes multilayer adsorption on a heterogeneous surface. The linear form of Langmuir equation is:

$$\frac{C_e}{Q_e} = \frac{C_e}{Q_m} + \frac{1}{K_L Q_m}$$

where Q_e is the equilibrium adsorption capacity of adsorbent, C_e is the equilibrium concentration of adsorbate, Q_m is the maximum adsorption capacity corresponding to complete monolayer coverage on the adsorbent surface, and K_L is a constant related to the energy of adsorption. The feasibility of the adsorption process is determined by R_L, which is given as [171–173]:

$$R_L = \frac{1}{1 + K_L C_0}$$

where C_0 is the initial concentration of adsorbate, and R_L is known as the separation factor and is dimensionless. If R_L is between 0 and 1, a favorable isotherm is represented, which means an effective interaction between the adsorbent and adsorbate. If R_L is greater than 1, an unfavorable isotherm is implied. If R_L equals 1, a linear isotherm is meant, and if R_L equals 0, an irreversible isotherm is indicated.

The linear form of Freundlich isotherm can be expressed as follows:

$$\log Q_e = \log K_F + \frac{1}{n} \log C_e$$

where Q_e is the equilibrium adsorption capacity of adsorbent, C_e is the equilibrium concentration of adsorbate, and K_F and n are Freundlich constants related to the adsorption capacity and intensity, respectively. A favorable adsorption has an n between 1 and 10; a normal L-type isotherm is represented when $1/n < 1$, which means an effective interaction between the adsorbent and adsorbate; if $1/n > 1$, a co-adsorption is implied [174–177].

Zhou et al. [164] prepared sponge-like polysiloxane-GO gel via a simple one-step sol-gel method to remove Pb(II) and Cd(II) from wastewater. Dubinin-Radushkevish isotherm was employed to confirm that chemisorption occurred. Temkin isotherm assumes that the heat of adsorption decreases linearly rather than logarithmic with coverage. Instead of pure GO, Verma et al. [120] utilized ammonia-modified GO to enhance its adsorption selectivity towards U(VI), and the adsorption capacity was in good agreement with the Temkin model. Redlich-Peterson isotherm is a hybrid of the Langmuir and Freundlich isotherms. Najafabadi et al. [122] fabricated a chitosan/GO composite nanofibrous adsorbent through electrospinning for removal of Cu(II), Pb(II), and Cr(VI) from an aqueous solution. It was found that the Redlich-Peterson isotherm model fitted better than the Langmuir and Freundlich models. Sips isotherm is also called Langmuir-Freundlich isotherm. It is a combination of the Langmuir and Freundlich isotherms. At low adsorbate concentrations, it reduces to the Freundlich isotherm, while at high concentrations, it approaches the monolayer adsorption capacity like the Langmuir isotherm. A poly(sodium acrylate)-GO (PSA–GO) double network hydrogel adsorbent was prepared by Xu et al. and used to adsorb Cd(II) and Mn(II) [125]. The adsorption process could be best described by the Sips model. Henry isotherm is the simplest adsorption isotherm in that the equilibrium adsorption capacities are proportional to the adsorbate concentrations. It is typically taken as valid for low surface coverages. Guo et al. [105] synthesized amino functionalized magnetic graphene composites and studied their performance for adsorbing Cr(VI), Pb(II), Hg(II), Cd(II), and Ni(II) from an aqueous solution. The adsorption of Cr(VI) and Pb(II) was well fitted with the Henry model.

The most commonly used adsorption kinetic models are pseudo-first-order and pseudo-second-order models. Their linear equation forms are given as follows:

$$\log(Q_e - Q_t) = \log(Q_e) - \left(\frac{k_1}{2.303}\right) t$$

$$\frac{t}{Q_t} = \frac{1}{k_2 Q_e^2} + \left(\frac{1}{Q_e}\right) t$$

where Q_e and Q_t are the adsorption capacities at equilibrium time and time t, respectively; k_1 and k_2 are the pseudo-first-order rate constant and pseudo-second-order rate constant, respectively. Pseudo-second-order model hypothesizes that the rate-limiting step is chemical adsorption involving valence forces through sharing or exchange of electrons between the adsorbent and adsorbate.

Tan et al. [167] prepared highly ordered layered GO membranes with larger interlayer spacing by an induced directional flow method and used them for removal of Cu(II), Cd(II), and Ni(II) from an aqueous solution. The kinetic data was consistent with intraparticle diffusion model, which meant that adsorption of those adsorbates onto the GO membranes included both external and intra-particle diffusion, and the intra-particle diffusion was not the only rate-limiting step. A magnetic biochar was synthesized by Wang et al. to adsorb As(V) from an aqueous solution, and Elovich model gave a good simulation result, which suggested that multiple interaction mechanisms or processes might control the adsorption of As(V) [169]. Cui et al. [123] fabricated magnetic carbonate hydroxyapatite/GO (M-CHAP/GO) and studied its Pb(II) removal abilities. Pseudo-first-order, pseudo-second-order, Elovich, intraparticle diffusion, and Bangham equations were applied to the description of adsorption kinetics, respectively. The pseudo-second-order model fitted best, and therefore, the main rate determining step was chemisorptions. In other words, the adsorption rate was controlled by chemical process through electronic exchange or chemical reactions between the M-CHAP/GO and Pb(II).

3.2.2 Interactions between adsorbents and adsorbates

It's important to understand the mechanism for adsorption of metals by adsorbents, which plays a significant role in designing more effective adsorbents. The interactions between adsorbents and adsorbates mainly include electrostatic interaction, ion exchange, complex formation, and redox reaction [160, 161].

Yang et al. [134] utilized magnetic Prussian blue/GO (PB/Fe_3O_4/GO) nanocomposites to adsorb radioactive Cs(I) in water, which were synthesized by an in situ controllable method. It was found that the concentration of hydrogen ions obviously increased after adsorption, and the increased value was greater than the reduced amount of Cs(I). Thus, the mechanism for adsorption of Cs(I) onto PB/Fe_3O_4/GO may be H^+-exchange and/or ion trapping. Zhou et al. [141] synthesized chitosan-functionalized MWCNT/$CoFe_2O_4$-NH_2 (MNP-CTS) hybrid material for the removal of Pb(II). After the adsorption of Pb(II), the peak of N-H bond in the FTIR spectra of MNP-CTS shifted from 1558 to 1575 cm^{-1}, which was attributed to the formation of stable complexes between Pb(II) and nitrogen in amine groups. Moreover, the peaks of C-O groups at 1071 and 1191 cm^{-1} shifted to 1043 and 1079 cm^{-1}, respectively, and it was thought to be caused by the chelating and ion exchange between Pb(II) and O-H groups. Dinda et al. [99] polymerized 2,6-diamino pyridine on GO surfaces via mutual oxidation-reduction techniques to prepare sulfuric acid-doped poly diaminopyridine/graphene (G-PDAP) composite. The as-prepared P-DAP was investigated as an adsorbent to remove high concentration of toxic Cr(VI) from water. It was confirmed that the mechanisms for removal of Cr(VI) mainly included reduction of Cr(VI) to Cr(III) at low pH and anion exchange between mobile dopant and chromate ions at high pH levels. Cui et al. [135] successfully anchored ethylenediaminetetraacetic acid (EDTA) on Fe_3O_4 nanoparticles functionalized GO to obtain EDTA functionalized magnetic GO (GO-Fe_3O_4-EDTA) for the first time. The synthesized GO-Fe_3O_4-EDTA displayed excellent adsorption performance for Pb(II), Hg(II), and Cu(II). EDTA was believed to have a strong coordination interaction with metal ions. In addition, ζ potential analysis illustrated that the surface of GO-Fe_3O_4-EDTA was electronegative and the oxygenic functional groups on GO surface were deprotonated, which indicated that electrostatic attraction may be another reason for Pb(II), Hg(II), and Cu(II) binding to the GO-Fe_3O_4-EDTA.

4 Practical application

The environmental water samples are far more complex than that prepared in the laboratory due to some known or unknown substances, such as various metals, organics, and microorganisms. That an adsorbent performs very well in the laboratory cannot ensure its applicability to real water. Normally, the performance of an adsorbent decreases to some extent when it is used in practice. However, many modified carbon nanomaterials still show excellent adsorption ability in spite of those interfering substances in real water, which obviously demonstrates their practicality.

Chen et al. [133] attached polyethyleneimine (PEI) to the GO through an amidation reaction between the amine groups of PEI and the carboxyl groups of GO, which could not only effectively prevent the agglomeration of GO nanosheets but also greatly enhance its adsorption performance for metal ions. The prepared PEI-GO composite showed a much higher maximum uptake capacity for Cr(VI) than many other conventional adsorbents, such as ethylenediamine-functionalized Fe_3O_4, PVP-modified activated carbon, mesoporous TiO_2, polypyrrole/Fe_3O_4 nanocomposite, hierarchical porous carbon, and chitosan-Fe(III) complex. Moreover, a removal percentage of 96.4% was observed after the PEI-GO at a concentration of 0.01 g/L was applied to the electroplating wastewater (Zhangzhou electroplating factory, China) spiked with 11.0 mg/L Cr(VI). It was evident that coexisting ions in electroplating wastewater had a weak influence on the adsorption of Cr(VI) onto PEI-GO. Aliyari et al. [55] reported the

synthesis and application of diethylenetriamine-functionalized magnetic GO nanocomposites (GO-Fe_3O_4-DETA) as an adsorbent for the simultaneous separation and preconcentration of Pb(II) and Cd(II) from real water and vegetable samples prior to their determination by flame atomic absorption spectrometry. Sea water (the Caspian sea), river water (the Babolrud river), well water (a well in Tehran), treated lettuce, celery, and potato samples were investigated, respectively. More than 94% of Pb(II) and Cd(II) in those real samples were recovered and the relative standard deviations were less than 3.5%, which clearly demonstrated the practical applicability of GO-Fe_3O_4-DETA nanocomposites. Shaheen et al. [76] achieved the selective adsorption of Au(III) from an aqueous solution containing such interfering ions as Zn(II), Mn(II), Pb(II), and Cd(II) using oxidized MWCNTs (o-MWCNTs) that were prepared by oxidation of MWCNTs. The o-MWCNTs were also applied to real environmental water samples, including tap water collected from the laboratory, ground water and sea water collected from Jeddah city (Saudi Arabia), treated wastewater collected from the wastewater treatment station at King Abdulaziz University, and finally drinking water (Aquafina bottled water). All those real samples were spiked with Au(III) at the concentrations of 2, 5, and 10 mg/L, respectively, and the o-MWCNTs were kept at 0.4 mg/mL in them. The results exhibited that almost all the Au(III) were removed, which indicated that the o-MWCNTs were quite reliable, feasible, and suitable for the selective adsorption of Au(III) from real water samples. Ensafi et al. [73] oxidized and modified MWCNTs with concentrated HNO_3 and thiolated cyanuric acid, respectively, and the treated MWCNTs were employed as adsorbents for the separation and preconcentration of Cd(II) and Pb(II) in various water samples, such as river water from the Zayandeh-Roud river (Isfahan, Iran), industrial wastewater (Mobarake Steel Complex, Isfahan, Iran), tap water, radiator manufacturing wastewater, and rice sample solution. The results showed a quite high recovery percentage of Cd(II) and Pb(II). Zhou et al. [75] used MWCNTs as the adsorbent and sodium diethyldithiocarbamate as the chelating agent for the simultaneous enrichment of Ni(II), Co(II), and Hg(II) in river water, sewage water, and factory water, respectively, and satisfied results were achieved.

5 Conclusions and prospects

It is of the utmost importance that water is clean and safe to use. However, water pollution is a serious problem around the world, especially in the developing countries. Millions of people are suffering from the threats of unhealthy water. Adsorption technologies are regarded as some of the most prevailing devices to mitigate water challenges, since they make it possible to supply clean water while being low cost and having a low energy consumption. Carbon-based nanomaterials as adsorbents have gained much attention in recent years due to their high stable structures, unique properties, and outstanding removal performances. Different types of modified carbon nanoadsorbents and their adsorption performances, common methods to modify carbon nanomaterials, various adsorption isotherm and kinetic models, diverse adsorption mechanisms, and practical applications of the modified carbon nanoadsorbents are covered. Currently, most research focuses on graphene- and CNT-based nanoadsorbents. Adsorption behaviors are best described by Langmuir or Freundlich isotherm models in most cases, and pseudo-first order or pseudo-second-order models are often more suitable for simulating adsorption kinetics than others. Adsorption mechanisms mainly include electrostatic interaction, ion exchange, complex formation, and redox reaction, and lots of modified carbon nanoadsorbents not only perform very well in laboratories but exhibit excellent applicability to real environmental water.

There are many factors affecting the adsorption performance of an adsorbent, such as its surface area, porosity, size, shape, composition, and functional groups. All of them can be utilized to optimize an adsorbent either by increasing the number and density of adsorption sites or by enhancing the interaction between adsorbents and adsorbates. Through analyzing the modification methods, functionalizing carbon nanomaterials with polymers, especially for those polymers containing electron-donating atoms, is becoming a very prevalent and promising way to improve their adsorption abilities due to the convenience in tailoring the molecular structures and properties of polymers. In order to facilitate the recovery of adsorbents after adsorption, making carbon nanomaterials magnetic is a more and more popular method owing to such characteristics of magnetic separation as easy to operate, economical, and environmentally friendly.

In short, many superior carbon-based nanoadsorbents have been developed that not only exhibit outstanding adsorption capacity and rate but allow for easy recovery. They have very promising uses in practice. However, there are still some issues to concern. Adsorbents with a high selectivity towards a particular metal need to be further developed. There are fewer reports that carbon-based nanoadsorbents can remove targeted metals in the presence of large quantities of other metals, especially when the coexisted metals are similar to the targeted ones. High-performance carbon-based nanoadsorbents that can achieve the removal of trace metals from aqueous solutions also need further development. In many cases, the concentrations of metals are extremely low and only a little higher than their maximum levels in drinking water. However, most adsorbents do not perform well for this concentration range. Moreover, the potential impacts of carbon-based nanomaterials on ecological and biological systems are rarely involved. The carbon-based nanoadsorbents can hardly be

completely recovered or removed from the solution after adsorption. It is urgently needed to improve the ability of recovering or removing them by such methods as precipitation and filtration or to incorporate low toxic or non-toxic materials to reduce their toxicity, like biomass and polymers. In addition, there needs to investigate the technical and economical feasibilities of their mass production. Hopefully these issues can be paid attention to in the future work.

Compliance with ethical standards

Conflict of interest The authors declare that they have no conflict of interest.

References

1. Trujillo-Reyes J, Peralta-Videa JR, Gardea-Torresdey JL (2014) Supported and unsupported nanomaterials for water and soil remediation: are they a useful solution for worldwide pollution? J Hazard Mater 280:487–503. https://doi.org/10.1016/j.jhazmat.2014.08.029
2. Wujcik EK, Londono NJ, Duirk SE, Monty CN, Masel RI (2013) An acetylcholinesterase-inspired biomimetic toxicity sensor. Chemosphere 91(8):1176–1182. https://doi.org/10.1016/j.chemosphere.2013.01.027
3. Wujcik EK, Duirk SE, Chase GG, Monty CN (2016) A visible colorimetric sensor based on nanoporous polypropylene fiber membranes for the determination of trihalomethanes in treated drinking water. Sensors Actuators B Chem 223:1–8. https://doi.org/10.1016/j.snb.2015.09.004
4. Fialova D, Kremplova M, Melichar L, Kopel P, Hynek D, Adam V, Kizek R (2014) Interaction of heavy metal ions with carbon and iron based particles. Materials 7(3):2242–2256. https://doi.org/10.3390/ma7032242
5. Olanipekun O, Oyefusi A, Neelgund GM, Oki A (2014) Adsorption of lead over graphite oxide. Spectrochim Acta A Mol Biomol Spectrosc 118:857–860. https://doi.org/10.1016/j.saa.2013.09.088
6. Shirani M, Semnani A, Habibollahi S, Haddadi H (2015) Ultrasound-assisted, ionic liquid-linked, dual-magnetic multiwall carbon nanotube microextraction combined with electrothermal atomic absorption spectrometry for simultaneous determination of cadmium and arsenic in food samples. J Anal At Spectrom 30(5):1057–1063. https://doi.org/10.1039/c4ja00481g
7. Aceto SR, Lu Y, Narayanan R, Heskett D, Wujcik EK, Bose A (2017) Hexagonally patterned mixed surfactant-templated room temperature synthesis of titania-lead selenide nanocomposites. Adv Compos & Hy Matls (in press)
8. Sharma A, Sharma A, Arya RK (2014) Removal of mercury(II) from aqueous solution: a review of recent work. Sep Sci Technol 50(9):1310–1320. https://doi.org/10.1080/01496395.2014.968261
9. National Primary Drinking Water Regulations (2017) United States Environmental Protection Agency. https://www.epa.gov/ground-water-and-drinking-water/national-primary-drinking-water-regulations. Accessed 17 May 2017
10. Zhu J, Wei S, Gu H, Rapole SB, Wang Q, Luo Z, Haldolaarachchige N, Young DP, Guo Z (2012) One-pot synthesis of magnetic graphene nanocomposites decorated with core@double-shell nanoparticles for fast chromium removal. Environ Sci Technol 46(2):977–985. https://doi.org/10.1021/es2014133
11. Imamoglu M, Tekir O (2008) Removal of copper (II) and lead (II) ions from aqueous solutions by adsorption on activated carbon from a new precursor hazelnut husks. Desalination 228(1–3):108–113. https://doi.org/10.1016/j.desal.2007.08.011
12. Rengaraj S, Joo CK, Kim Y, Yi J (2003) Kinetics of removal of chromium from water and electronic process wastewater by ion exchange resins: 1200H, 1500H and IRN97H. J Hazard Mater 102(2–3):257–275. https://doi.org/10.1016/s0304-3894(03)00209-7
13. Dabrowski A, Hubicki Z, Podkoscielny P, Robens E (2004) Selective removal of the heavy metal ions from waters and industrial wastewaters by ion-exchange method. Chemosphere 56(2):91–106. https://doi.org/10.1016/j.chemosphere.2004.03.006
14. Modrzejewska Z, Kaminski W (1999) Separation of Cr(VI) on chitosan membranes. Ind Eng Chem Res 38:4946–4950. https://doi.org/10.1021/ie980612g
15. Qdais HA, Moussa H (2004) Removal of heavy metals from wastewater by membrane processes: a comparative study. Desalination 164:105–110
16. Kongsricharoern N, Polprasert C (1996) Chromium removal by a bipolar electro-chemical precipitation process. Wat Sci Tech 34(9):109–116
17. Hunsom M, Pruksathorn K, Damronglerd S, Vergnes H, Duverneuil P (2005) Electrochemical treatment of heavy metals (Cu^{2+}, Cr^{6+}, Ni^{2+}) from industrial effluent and modeling of copper reduction. Water Res 39(4):610–616. https://doi.org/10.1016/j.watres.2004.10.011
18. Dialynas E, Diamadopoulos E (2009) Integration of a membrane bioreactor coupled with reverse osmosis for advanced treatment of municipal wastewater. Desalination 238:302–311. https://doi.org/10.1016/j.desal.200
19. Mohsen-Nia M, Montazeri P, Modarress H (2007) Removal of Cu^{2+} and Ni^{2+} from wastewater with a chelating agent and reverse osmosis processes. Desalination 217(1–3):276–281. https://doi.org/10.1016/j.desal.2006.01.043
20. Fu F, Wang Q (2011) Removal of heavy metal ions from wastewaters: a review. J Environ Manag 92(3):407–418. https://doi.org/10.1016/j.jenvman.2010.11.011
21. Karbassi AR, Ayaz GO (2007) Flocculation of Cu, Zn, Pb, Ni and Mn during mixing of Talar River water with Caspian seawater. Int J Environ Res 1(1):66–73
22. Kumar R, Chawla J, Kaur I (2015) Removal of cadmium ion from wastewater by carbon-based nanosorbents: a review. J Water Health 13(1):18–33. https://doi.org/10.2166/wh.2014.024
23. Ghasemzadeh G, Momenpour M, Omidi F, Hosseini MR, Ahani M, Barzegari A (2014) Applications of nanomaterials in water treatment and environmental remediation. Front Environ Sci Eng 8(4):471–482. https://doi.org/10.1007/s11783-014-0654-0
24. Wu Y, Ma X, Feng M, Liu M (2008) Behavior of chromium and arsenic on activated carbon. J Hazard Mater 159(2–3):380–384. https://doi.org/10.1016/j.jhazmat.2008.02.059
25. Sitko R, Turek E, Zawisza B, Malicka E, Talik E, Heimann J, Gagor A, Feist B, Wrzalik R (2013) Adsorption of divalent metal ions from aqueous solutions using graphene oxide. Dalton Trans 42(16):5682–5689. https://doi.org/10.1039/c3dt33097d
26. Hua M, Zhang S, Pan B, Zhang W, Lv L, Zhang Q (2012) Heavy metal removal from water/wastewater by nanosized metal oxides: a review. J Hazard Mater 211-212:317–331. https://doi.org/10.1016/j.jhazmat.2011.10.016
27. Zhang G-S, Qu J-H, Liu H-J, Liu R-P, Li G-T (2007) Removal mechanism of As(III) by a novel Fe-Mn binary oxide adsorbent: oxidation and sorption. Environ Sci Technol 41:4613–4619. https://doi.org/10.1021/es063010u

28. Abollino O, Aceto M, Malandrino M, Sarzanini C, Mentasti E (2003) Adsorption of heavy metals on Na-montmorillonite. Effect of pH and organic substances. Water Res 37(7):1619–1627. https://doi.org/10.1016/s0043-1354(02)00524-9
29. Manohar DM, Krishnan KA, Anirudhan TS (2002) Removal of mercury(II) from aqueous solutions and chlor-alkali industry wastewater using 2-mercaptobenzimidazole-clay. Water Res 36: 1609–1619
30. Oliveira LC, Petkowicz DI, Smaniotto A, Pergher SB (2004) Magnetic zeolites: a new adsorbent for removal of metallic contaminants from water. Water Res 38(17):3699–3704. https://doi.org/10.1016/j.watres.2004.06.008
31. Erdem E, Karapinar N, Donat R (2004) The removal of heavy metal cations by natural zeolites. J Colloid Interface Sci 280(2): 309–314. https://doi.org/10.1016/j.jcis.2004.08.028
32. Hsu LC, Wang SL, Lin YC, Wang MK, Chiang PN, Liu JC, Kuan WH, Chen CC, Tzou YM (2010) Cr(VI) removal on fungal biomass of Neurospora crassa: the importance of dissolved organic carbons derived from the biomass to Cr(VI) reduction. Environ Sci Technol 44:6202–6208. https://doi.org/10.1021/es1017015
33. Loukidou MX, Matis KA, Zouboulis AI, Liakopoulou-Kyriakidou M (2003) Removal of As(V) from wastewaters by chemically modified fungal biomass. Water Res 37(18):4544–4552. https://doi.org/10.1016/s0043-1354(03)00415-9
34. Gu H, Rapole SB, Sharma J, Huang Y, Cao D, Colorado HA, Luo Z, Haldolaarachchige N, Young DP, Walters B, Wei S, Guo Z (2012) Magnetic polyaniline nanocomposites toward toxic hexavalent chromium removal. RSC Adv 2(29):11007–11018. https://doi.org/10.1039/c2ra21991c
35. Qiu B, Xu C, Sun D, Yi H, Guo J, Zhang X, Qu H, Guerrero M, Wang X, Noel N, Luo Z, Guo Z, Wei S (2014) Polyaniline coated ethyl cellulose with improved hexavalent chromium removal. ACS Sustain Chem Eng 2(8):2070–2080. https://doi.org/10.1021/sc5003209
36. Khan MA, Gee E, Choi J, Kumar M, Jung W, Timmes TC, Kim H-C, Jeon B-H (2013) Adsorption of cobalt onto graphite nanocarbon-impregnated alginate beads: equilibrium, kinetics, and thermodynamics studies. Chem Eng Commun 201(3):403–418. https://doi.org/10.1080/00986445.2013.773426
37. Qu J, Zhang Q, Xia Y, Cong Q, Luo C (2015) Synthesis of carbon nanospheres using fallen willow leaves and adsorption of Rhodamine B and heavy metals by them. Environ Sci Pollut Res Int 22(2):1408–1419. https://doi.org/10.1007/s11356-014-3447-x
38. Chen B, Ma Q, Tan C, Lim TT, Huang L, Zhang H (2015) Carbon-based sorbents with three-dimensional architectures for water remediation. Small 11(27):3319–3336. https://doi.org/10.1002/smll.201403729
39. Shen Y, Fang Q, Chen B (2015) Environmental applications of three-dimensional graphene-based macrostructures: adsorption, transformation, and detection. Environ Sci Technol 49(1):67–84. https://doi.org/10.1021/es504421y
40. Alijani H, Beyki MH, Shariatinia Z, Bayat M, Shemirani F (2014) A new approach for one step synthesis of magnetic carbon nanotubes/diatomite earth composite by chemical vapor deposition method: application for removal of lead ions. Chem Eng J 253:456–463. https://doi.org/10.1016/j.cej.2014.05.021
41. Ray PZ, Shipley HJ (2015) Inorganic nano-adsorbents for the removal of heavy metals and arsenic: a review. RSC Adv 5(38): 29885–29907. https://doi.org/10.1039/c5ra02714d
42. Khan MA, Jung W, Kwon O-H, Jung YM, Paeng K-J, Cho S-Y, Jeon B-H (2014) Sorption studies of manganese and cobalt from aqueous phase onto alginate beads and nano-graphite encapsulated alginate beads. J Ind Eng Chem 20(6):4353–4362. https://doi.org/10.1016/j.jiec.2014.01.043
43. Taghizadeh M, Asgharinezhad AA, Samkhaniany N, Tadjarodi A, Abbaszadeh A, Pooladi M (2014) Solid phase extraction of heavy metal ions based on a novel functionalized magnetic multi-walled carbon nanotube composite with the aid of experimental design methodology. Microchim Acta 181(5–6):597–605. https://doi.org/10.1007/s00604-013-1154-9
44. Chowdhury S, Balasubramanian R (2014) Recent advances in the use of graphene-family nanoadsorbents for removal of toxic pollutants from wastewater. Adv Colloid Interf Sci 204:35–56. https://doi.org/10.1016/j.cis.2013.12.005
45. Zhao L, Yu B, Xue F, Xie J, Zhang X, Wu R, Wang R, Hu Z, Yang ST, Luo J (2015) Facile hydrothermal preparation of recyclable S-doped graphene sponge for Cu2+ adsorption. J Hazard Mater 286: 449–456. https://doi.org/10.1016/j.jhazmat.2015.01.021
46. Lei Y, Chen F, Luo Y, Zhang L (2014) Synthesis of three-dimensional graphene oxide foam for the removal of heavy metal ions. Chem Phys Lett 593:122–127. https://doi.org/10.1016/j.cplett.2013.12.066
47. Xie L, Jiang R, Zhu F, Liu H, Ouyang G (2014) Application of functionalized magnetic nanoparticles in sample preparation. Anal Bioanal Chem 406(2):377–399. https://doi.org/10.1007/s00216-013-7302-6
48. Lan Y, Liu H, Cao X, Zhao S, Dai K, Yan X, Zheng G, Liu C, Shen C, Guo Z (2016) Electrically conductive thermoplastic polyurethane/polypropylene nanocomposites with selectively distributed graphene. Polymer 97:11–19. https://doi.org/10.1016/j.polymer.2016.05.017
49. Yan L, Zhao Q, Jiang T, Liu X, Li Y, Fang W, Yin H (2015) Adsorption characteristics and behavior of a graphene oxide-Al13 composite for cadmium ion removal from aqueous solutions. RSC Adv 5(83):67372–67379. https://doi.org/10.1039/c5ra10174c
50. Zhu J, Chen M, Qu H, Luo Z, Wu S, Colorado HA, Wei S, Guo Z (2013) Magnetic field induced capacitance enhancement in graphene and magnetic graphene nanocomposites. Energy Environ Sci 6(1):194–204. https://doi.org/10.1039/c2ee23422j
51. Liu H, Dong M, Huang W, Gao J, Dai K, Guo J, Zheng G, Liu C, Shen C, Guo Z (2017) Lightweight conductive graphene/thermoplastic polyurethane foams with ultrahigh compressibility for piezoresistive sensing. J Mater Chem C 5(1):73–83. https://doi.org/10.1039/c6tc03713e
52. Xu T, Chen L, Guo Z, Ma T (2016) Strategic improvement of the long-term stability of perovskite materials and perovskite solar cells. Phys Chem Chem Phys 18(39):27026–27050. https://doi.org/10.1039/c6cp04553g
53. Wei H, Gu H, Guo J, Yan X, Liu J, Cao D, Wang X, Wei S, Guo Z (2017) Significantly enhanced energy density of magnetite/polypyrrole nanocomposite capacitors at high rates by low magnetic fields. Adv Compos & Hy Matls (in press)
54. Liu H, Gao J, Huang W, Dai K, Zheng G, Liu C, Shen C, Yan X, Guo J, Guo Z (2016) Electrically conductive strain sensing polyurethane nanocomposites with synergistic carbon nanotubes and graphene bifillers. Nano 8(26):12977–12989. https://doi.org/10.1039/C6NR02216B
55. Aliyari E, Alvand M, Shemirani F (2015) Simultaneous separation and preconcentration of lead and cadmium from water and vegetable samples using a diethylenetriamine-modified magnetic graphene oxide nanocomposite. Anal Methods 7(18):7582–7589. https://doi.org/10.1039/c5ay01088h
56. Gu Y, Sun Y, Zhang Y, Chi H, Zhang W, Liang Q, Jing R (2014) Highly efficient adsorption of copper ions by a PVP-reduced graphene oxide based on a new adsorptions mechanism. Nano-Micro Lett 6(1):80–87. https://doi.org/10.1007/bf03353772
57. Dong Z, Wang D, Liu X, Pei X, Chen L, Jin J (2014) Bio-inspired surface-functionalization of graphene oxide for the adsorption of organic dyes and heavy metal ions with a superhigh capacity. J Mater Chem A 2(14):5034–5040. https://doi.org/10.1039/c3ta14751g

58. Gopalakrishnan A, Krishnan R, Thangavel S, Venugopal G, Kim S-J (2015) Removal of heavy metal ions from pharma-effluents using graphene-oxide nanosorbents and study of their adsorption kinetics. J Ind Eng Chem 30:14–19. https://doi.org/10.1016/j.jiec.2015.06.005
59. Li L, Wang Z, Ma P, Bai H, Dong W, Chen M (2015) Preparation of polyvinyl alcohol/chitosan hydrogel compounded with graphene oxide to enhance the adsorption properties for Cu(II) in aqueous solution. J Polym Res 22(8):150. https://doi.org/10.1007/s10965-015-0794-3
60. Jiang T, Yan L, Zhang L, Li Y, Zhao Q, Yin H (2015) Fabrication of a novel graphene oxide/β-FeOOH composite and its adsorption behavior for copper ions from aqueous solution. Dalton Trans 44(22):10448–10456. https://doi.org/10.1039/c5dt01030f
61. Olanipekun O, Oyefusi A, Neelgund GM, Oki A (2015) Synthesis and characterization of reduced graphite oxide-polymer composites and their application in adsorption of lead. Spectrochim Acta A Mol Biomol Spectrosc 149:991–996. https://doi.org/10.1016/j.saa.2015.04.071
62. Cheng C, Liu Z, Li X, Su B, Zhou T, Zhao C (2014) Graphene oxide interpenetrated polymeric composite hydrogels as highly effective adsorbents for water treatment. RSC Adv 4(80):42346–42357. https://doi.org/10.1039/c4ra07114j
63. Ding Z, Hu X, Morales VL, Gao B (2014) Filtration and transport of heavy metals in graphene oxide enabled sand columns. Chem Eng J 257:248–252. https://doi.org/10.1016/j.cej.2014.07.034
64. Gu D, Fein JB (2015) Adsorption of metals onto graphene oxide: surface complexation modeling and linear free energy relationships. Colloids Surf A Physicochem Eng Asp 481:319–327. https://doi.org/10.1016/j.colsurfa.2015.05.026
65. Dong Z, Zhang F, Wang D, Liu X, Jin J (2015) Polydopamine-mediated surface-functionalization of graphene oxide for heavy metal ions removal. J Solid State Chem 224:88–93. https://doi.org/10.1016/j.jssc.2014.06.030
66. Deng D, Jiang X, Yang L, Hou X, Zheng C (2014) Organic solvent-free cloud point extraction-like methodology using aggregation of graphene oxide. Anal Chem 86(1):758–765. https://doi.org/10.1021/ac403345s
67. Xu Z, Zhang Y, Qian X, Shi J, Chen L, Li B, Niu J, Liu L (2014) One step synthesis of polyacrylamide functionalized graphene and its application in Pb(II) removal. Appl Surf Sci 316:308–314. https://doi.org/10.1016/j.apsusc.2014.07.155
68. Santhana KKA, Jiang S-J (2015) Preparation and characterization of exfoliated graphene oxide-L-cystine as an effective adsorbent of Hg(II) adsorption. RSC Adv 5(9):6294–6304. https://doi.org/10.1039/c4ra12564a
69. Wen T, Wu X, Liu M, Xing Z, Wang X, Xu AW (2014) Efficient capture of strontium from aqueous solutions using graphene oxide-hydroxyapatite nanocomposites. Dalton Trans 43(20):7464–7472. https://doi.org/10.1039/c3dt53591f
70. Yang J, Wu J-X, Lü Q-F, Lin T-T (2014) Facile preparation of lignosulfonate-graphene oxide-polyaniline ternary nanocomposite as an effective adsorbent for Pb(II) ions. ACS Sustain Chem Eng 2(5):1203–1211. https://doi.org/10.1021/sc500030v
71. Mubarak NM, Sahu JN, Abdullah EC, Jayakumar NS (2013) Removal of heavy metals from wastewater using carbon nanotubes. Separation & Purification Reviews 43(4):311–338. https://doi.org/10.1080/15422119.2013.821996
72. Ensafi AA, Jokar M, Ghiaci M (2014) Modified multiwall carbon nanotubes supported on graphite as a suitable solid nano-sorbent for selective separation and preconcentration of trace amounts of cadmium and lead ions. J Iran Chem Soc 12(3):457–467. https://doi.org/10.1007/s13738-014-0503-x
73. Anitha K, Namsani S, Singh JK (2015) Removal of heavy metal ions using a functionalized single-walled carbon nanotube: a molecular dynamics study. J Phys Chem A 119(30):8349–8358. https://doi.org/10.1021/acs.jpca.5b03352
74. Zhou Q, Xing A, Zhao K (2014) Simultaneous determination of nickel, cobalt and mercury ions in water samples by solid phase extraction using multiwalled carbon nanotubes as adsorbent after chelating with sodium diethyldithiocarbamate prior to high performance liquid chromatography. J Chromatogr A 1360:76–81. https://doi.org/10.1016/j.chroma.2014.07.084
75. Zhang X, Huang Q, Liu M, Tian J, Zeng G, Li Z, Wang K, Zhang Q, Wan Q, Deng F, Wei Y (2015) Preparation of amine functionalized carbon nanotubes via a bioinspired strategy and their application in Cu2+ removal. Appl Surf Sci 343:19–27. https://doi.org/10.1016/j.apsusc.2015.03.081
76. Shaheen HA, Marwani HM, Soliman EM (2015) Selective adsorption of gold ions from complex system using oxidized multi-walled carbon nanotubes. J Mol Liq 212:480–486. https://doi.org/10.1016/j.molliq.2015.09.040
77. Ihsanullah, Al-Khaldi FA, Abusharkh B, Khaled M, Atieh MA, Nasser MS, Laoui T, Saleh TA, Agarwal S, Tyagi I, Gupta VK (2015) Adsorptive removal of cadmium(II) ions from liquid phase using acid modified carbon-based adsorbents. J Mol Liq 204:255–263. https://doi.org/10.1016/j.molliq.2015.01.033
78. Cai YQ, Yu GQ, Liu CD, Xu YY, Wang W (2012) Imidazolium ionic liquid-supported sulfonic acids: efficient and recyclable catalysts for esterification of benzoic acid. Chin Chem Lett 23(1):1–4. https://doi.org/10.1016/j.cclet.2011.09.016
79. Chawla J, Kumar R, Kaur I (2015) Carbon nanotubes and graphenes as adsorbents for adsorption of lead ions from water: a review. J Water Supply Res Technol AQUA 64(6):641–659. https://doi.org/10.2166/aqua.2015.102
80. Wujcik EK, Monty CN (2013) Nanotechnology for implantable sensors: carbon nanotubes and graphene in medicine. Wiley Interdiscip Rev Nanomed Nanobiotechnol 5(3):233–249. https://doi.org/10.1002/wnan.1213
81. Aqeel SM, Huanga Z, Walton J, Baker C, Falkner D, Liu Z, Wang Z (2017) Advanced functional polyvinylidene fluoride (PVDF)/polyacrilonitrile (PAN) organic semiconductor assisted by aligned nanocarbon toward energy storage and conversion. Adv Compos & Hy Matls (in press)
82. Zhan C, Yu G, Lu Y, Wang L, Wujcik E, Wei S (2017) Conductive polymer nanocomposites: a critical review of modern advanced devices. J Mater Chem C 5(7):1569–1585. https://doi.org/10.1039/c6tc04269d
83. Blasdel NJ, Wujcik EK, Carletta JE, Lee K-S, Monty CN (2015) Fabric nanocomposite resistance temperature detector. IEEE Sensors J 15(1):300–306. https://doi.org/10.1109/jsen.2014.2341915
84. Ge Y, Li Z, Xiao D, Xiong P, Ye N (2014) Sulfonated multi-walled carbon nanotubes for the removal of copper (II) from aqueous solutions. J Ind Eng Chem 20(4):1765–1771. https://doi.org/10.1016/j.jiec.2013.08.030
85. Nekouei S, Nekouei F (2014) Application of multiwalled carbon nanotubes modified by diethyl dithiophosphate ammonium for selective solid phase extraction of ultra traces Ni(II) and Co(II) in river water samples. Studia UBB Chemia 59(3):49–59
86. Wang Y, Gu Z, Yang J, Liao J, Yang Y, Liu N, Tang J (2014) Amidoxime-grafted multiwalled carbon nanotubes by plasma techniques for efficient removal of uranium(VI). Appl Surf Sci 320:10–20. https://doi.org/10.1016/j.apsusc.2014.08.182
87. Tian Z, Yang B, Cui G, Zhang L, Guo Y, Yan S (2015) Synthesis of poly(m-phenylenediamine)/iron oxide/acid oxidized multi-wall carbon nanotubes for removal of hexavalent chromium. RSC Adv 5(3):2266–2275. https://doi.org/10.1039/c4ra10282g
88. Wang Y, Shi L, Gao L, Wei Q, Cui L, Hu L, Yan L, Du B (2015) The removal of lead ions from aqueous solution by using magnetic hydroxypropyl chitosan/oxidized multiwalled carbon nanotubes

composites. J Colloid Interface Sci 451:7–14. https://doi.org/10.1016/j.jcis.2015.03.048
89. Wang Y, Wei H, Lu Y, Wei S, Wujcik E, Guo Z (2015) Multifunctional carbon nanostructures for advanced energy storage applications. Nano 5(2):755–777. https://doi.org/10.3390/nano5020755
90. Sharma J, Lizu M, Stewart M, Zygula K, Lu Y, Chauhan R, Yan X, Guo Z, Wujcik E, Wei S (2015) Multifunctional nanofibers towards active biomedical therapeutics. Polymers 7(2):186–219. https://doi.org/10.3390/polym7020186
91. Lu Y, Huang J, Yu G, Cardenas R, Wei S, Wujcik EK, Guo Z (2016) Coaxial electrospun fibers: applications in drug delivery and tissue engineering. Wiley Interdiscip Rev Nanomed Nanobiotechnol 8(5):654–677. https://doi.org/10.1002/wnan.1391
92. Qu H, Wei S, Guo Z (2013) Coaxial electrospun nanostructures and their applications. J Mater Chem A 1(38):11513–11528. https://doi.org/10.1039/c3ta12390a
93. Zhu J, Gu H, Guo J, Chen M, Wei H, Luo Z, Colorado HA, Yerra N, Ding D, Ho TC, Haldolaarachchige N, Hopper J, Young DP, Guo Z, Wei S (2014) Mesoporous magnetic carbon nanocomposite fabrics for highly efficient Cr(VI) removal. J Mater Chem A 2(7):2256–2265. https://doi.org/10.1039/c3ta13957c
94. Zhang X, Liu J, Kelly SJ, Huang X, Liu J (2014) Biomimetic snowflake-shaped magnetic micro−/nanostructures for highly efficient adsorption of heavy metal ions and organic pollutants from aqueous solution. J Mater Chem A 2:11759–11767. https://doi.org/10.1039/c4ta02058h
95. Qiu B, Gu H, Yan X, Guo J, Wang Y, Sun D, Wang Q, Khan M, Zhang X, Weeks BL, Young DP, Guo Z, Wei S (2014) Cellulose derived magnetic mesoporous carbon nanocomposites with enhanced hexavalent chromium removal. J Mater Chem A 2(41):17454–17462. https://doi.org/10.1039/c4ta04040f
96. Han C, Ma Q, Yang Y, Yang M, Yu W, Dong X, Wang J, Liu G (2015) Electrospinning-derived [C/Fe3O4]@C coaxial nanocables with tuned magnetism, electrical conduction and highly efficient adsorption trifunctionality. J Mater Sci Mater Electron 26(10):8054–8064. https://doi.org/10.1007/s10854-015-3463-8
97. Cui HJ, Cai JK, Zhao H, Yuan B, Ai C, Fu ML (2014) One step solvothermal synthesis of functional hybrid γ-Fe2O3/carbon hollow spheres with superior capacities for heavy metal removal. J Colloid Interface Sci 425:131–135. https://doi.org/10.1016/j.jcis.2014.03.049
98. Mamun AA, Ahmed YM, AlKhatib MFR, Jameel AT, AlSaadi MAHAR (2015) Lead sorption by carbon nanofibers grown on powdered activated carbon—kinetics and equilibrium. NANO: Brief Reports and Reviews 10(2):1550017. https://doi.org/10.1142/s1793292015500174
99. Dinda D, Saha SK (2015) Sulfuric acid doped poly diaminopyridine/graphene composite to remove high concentration of toxic Cr(VI). J Hazard Mater 291:93–101. https://doi.org/10.1016/j.jhazmat.2015.02.065
100. Chella S, Kollu P, Komarala EVPR, Doshi S, Saranya M, Felix S, Ramachandran R, Saravanan P, Koneru VL, Venugopal V, Jeong SK, Grace AN (2015) Solvothermal synthesis of MnFe2O4-graphene composite—investigation of its adsorption and antimicrobial properties. Appl Surf Sci 327:27–36. https://doi.org/10.1016/j.apsusc.2014.11.096
101. Gao H, Lv S, Dou J, Kong M, Dai D, Si C, Liu G (2015) The efficient adsorption removal of Cr(VI) by using Fe3O4 nanoparticles hybridized with carbonaceous materials. RSC Adv 5(74):60033–60040. https://doi.org/10.1039/c5ra10236g
102. Muthukrishnaraj A, Manokaran J, Vanitha M, Thiruvengadaravi KV, Baskaralingam P, Balasubramanian N (2014) Equilibrium, kinetic and thermodynamic studies for the removal of Zn(II) and Ni(II) ions using magnetically recoverable graphene/Fe3O4 composite. Desalin Water Treat 56(9):2485–2501. https://doi.org/10.1080/19443994.2014.963149
103. Santhosh C, Kollu P, Felix S, Velmurugan V, Jeong SK, Grace AN (2015) CoFe2O4 and NiFe2O4@graphene adsorbents for heavy metal ions—kinetic and thermodynamic analysis. RSC Adv 5(37):28965–28972. https://doi.org/10.1039/c5ra02905h
104. Zhang Y, Yan T, Yan L, Guo X, Cui L, Wei Q, Du B (2014) Preparation of novel cobalt ferrite/chitosan grafted with graphene composite as effective adsorbents for mercury ions. J Mol Liq 198:381–387. https://doi.org/10.1016/j.molliq.2014.07.043
105. Guo X, Du B, Wei Q, Yang J, Hu L, Yan L, Xu W (2014) Synthesis of amino functionalized magnetic graphenes composite material and its application to remove Cr(VI), Pb(II), Hg(II), Cd(II) and Ni(II) from contaminated water. J Hazard Mater 278:211–220. https://doi.org/10.1016/j.jhazmat.2014.05.075
106. Sahoo AK, Srivastava SK, Raul PK, Gupta AK, Shrivastava R (2014) Graphene nanocomposites of CdS and ZnS in effective water purification. J Nanopart Res 16(7):2473. https://doi.org/10.1007/s11051-014-2473-4
107. Santhosh C, Kollu P, Doshi S, Sharma M, Bahadur D, Vanchinathan MT, Saravanan P, Kim B-S, Grace AN (2014) Adsorption, photodegradation and antibacterial study of graphene-Fe3O4 nanocomposite for multipurpose water purification application. RSC Adv 4(54):28300–28308. https://doi.org/10.1039/c4ra02913e
108. Li J, Chen C, Zhu K, Wang X (2016) Nanoscale zero-valent iron particles modified on reduced graphene oxides using a plasma technique for Cd(II) removal. J Taiwan Inst Chem Eng 59:389–394. https://doi.org/10.1016/j.jtice.2015.09.010
109. Li J, Chen C, Zhang R, Wang X (2015) Nanoscale zero-valent iron particles supported on reduced graphene oxides by using a plasma technique and their application for removal of heavy-metal ions. Chem Asian J 10(6):1410–1417. https://doi.org/10.1002/asia.201500242
110. Zhou G, Xu X, Zhu W, Feng B, Hu J (2015) Dispersedly embedded loading of Fe3O4 nanoparticles into graphene nanosheets for highly efficient and recyclable removal of heavy metal ions. New J Chem 39(9):7355–7362. https://doi.org/10.1039/c5nj00897b
111. Zhang L, Tian Y, Guo Y, Gao H, Li H, Yan S (2015) Introduction of α-MnO2 nanosheets to NH2 graphene to remove Cr6+ from aqueous solutions. RSC Adv 5(55):44096–44106. https://doi.org/10.1039/c5ra04545b
112. Yang L, Li Z, Nie G, Zhang Z, Lu X, Wang C (2014) Fabrication of poly(o-phenylenediamine)/reduced graphene oxide composite nanosheets via microwave heating and their effective adsorption of lead ions. Appl Surf Sci 307:601–607. https://doi.org/10.1016/j.apsusc.2014.04.083
113. Zhang Y, Yan L, Xu W, Guo X, Cui L, Gao L, Wei Q, Du B (2014) Adsorption of Pb(II) and Hg(II) from aqueous solution using magnetic CoFe2O4-reduced graphene oxide. J Mol Liq 191:177–182. https://doi.org/10.1016/j.molliq.2013.12.015
114. Tayyebi A, Outokesh M, Moradi S, Doram A (2015) Synthesis and characterization of ultrasound assisted "graphene oxide-magnetite" hybrid, and investigation of its adsorption properties for Sr(II) and Co(II) ions. Appl Surf Sci 353:350–362. https://doi.org/10.1016/j.apsusc.2015.06.087
115. Zhao Z, Li J, Wen T, Shen C, Wang X, Xu A (2015) Surface functionalization graphene oxide by polydopamine for high affinity of radionuclides. Colloids Surf A Physicochem Eng Asp 482:258–266. https://doi.org/10.1016/j.colsurfa.2015.05.020
116. Ma S, Zhan S, Jia Y, Zhou Q (2015) Highly efficient antibacterial and Pb(II) removal effects of Ag-CoFe2O4-GO nanocomposite. ACS Appl Mater Interfaces 7(19):10576–10586. https://doi.org/10.1021/acsami.5b02209
117. Tan M, Liu X, Li W, Li H (2015) Enhancing sorption capacities for copper(II) and lead(II) under weakly acidic conditions by L-

tryptophan-functionalized graphene oxide. J Chem Eng Data 60(5):1469–1475. https://doi.org/10.1021/acs.jced.5b00015

118. Zhang F, Song Y, Song S, Zhang R, Hou W (2015) Synthesis of magnetite-graphene oxide-layered double hydroxide composites and applications for the removal of Pb(II) and 2,4-dichlorophenoxyacetic acid from aqueous solutions. ACS Appl Mater Interfaces 7(13):7251–7263. https://doi.org/10.1021/acsami.5b00433
119. Xing HT, Chen JH, Sun X, Huang YH, Su ZB, Hu SR, Weng W, Li SX, Guo HX, Wu WB, He YS, Li FM, Huang Y (2015) NH2-rich polymer/graphene oxide use as a novel adsorbent for removal of cu(II) from aqueous solution. Chem Eng J 263:280–289. https://doi.org/10.1016/j.cej.2014.10.111
120. Verma S, Dutta RK (2015) A facile method of synthesizing ammonia modified graphene oxide for efficient removal of uranyl ions from aqueous medium. RSC Adv 5(94):77192–77203. https://doi.org/10.1039/c5ra10555b
121. Liu Y, Luo C, Cui G, Yan S (2015) Synthesis of manganese dioxide/iron oxide/graphene oxide magnetic nanocomposites for hexavalent chromium removal. RSC Adv 5(67):54156–54164. https://doi.org/10.1039/c5ra06455d
122. Najafabadi HH, Irani M, Rad RL, Haratameh HA, Haririan I (2015) Removal of Cu2+, Pb2+ and Cr6+ from aqueous solutions using a chitosan/graphene oxide composite nanofibrous adsorbent. RSC Adv 5(21):16532–16539. https://doi.org/10.1039/c5ra01500f
123. Cui L, Wang Y, Hu L, Gao L, Du B, Wei Q (2015) Mechanism of Pb(II) and methylene blue adsorption onto magnetic carbonate hydroxyapatite/graphene oxide. RSC Adv 5(13):9759–9770. https://doi.org/10.1039/c4ra13009j
124. Sui N, Wang L, Wu X, Li X, Sui J, Xiao H, Liu M, Wan J, Yu WW (2015) Polyethylenimine modified magnetic graphene oxide nanocomposites for Cu2+ removal. RSC Adv 5(1):746–752. https://doi.org/10.1039/c4ra11669k
125. Xu R, Zhou G, Tang Y, Chu L, Liu C, Zeng Z, Luo S (2015) New double network hydrogel adsorbent: highly efficient removal of Cd(II) and Mn(II) ions in aqueous solution. Chem Eng J 275:179–188. https://doi.org/10.1016/j.cej.2015.04.040
126. Jiang T, Liu W, Mao Y, Zhang L, Cheng J, Gong M, Zhao H, Dai L, Zhang S, Zhao Q (2015) Adsorption behavior of copper ions from aqueous solution onto graphene oxide-CdS composite. Chem Eng J 259:603–610. https://doi.org/10.1016/j.cej.2014.08.022
127. Sitko R, Janik P, Feist B, Talik E, Gagor A (2014) Suspended aminosilanized graphene oxide nanosheets for selective preconcentration of lead ions and ultrasensitive determination by electrothermal atomic absorption spectrometry. ACS Appl Mater Interfaces 6(22):20144–20153. https://doi.org/10.1021/am505740d
128. Kumar S, Nair RR, Pillai PB, Gupta SN, Iyengar MA, Sood AK (2014) Graphene oxide-MnFe2O4 magnetic nanohybrids for efficient removal of lead and arsenic from water. ACS Appl Mater Interfaces 6(20):17426–17436. https://doi.org/10.1021/am504826q
129. Jia W, Lu S (2014) Few-layered graphene oxides as superior adsorbents for the removal of Pb(II) ions from aqueous solutions. Korean J Chem Eng 31(7):1265–1270. https://doi.org/10.1007/s11814-014-0045-z
130. Lei Y, Chen F, Luo Y, Zhang L (2014) Three-dimensional magnetic graphene oxide foam/Fe3O4 nanocomposite as an efficient absorbent for Cr(VI) removal. J Mater Sci 49(12):4236–4245. https://doi.org/10.1007/s10853-014-8118-2
131. Fang F, Kong L, Huang J, Wu S, Zhang K, Wang X, Sun B, Jin Z, Wang J, Huang XJ, Liu J (2014) Removal of cobalt ions from aqueous solution by an amination graphene oxide nanocomposite. J Hazard Mater 270:1–10. https://doi.org/10.1016/j.jhazmat.2014.01.031
132. Li H, Chi Z, Li J (2013) Covalent bonding synthesis of magnetic graphene oxide nanocomposites for Cr(III) removal. Desalin Water Treat 52(10–12):1937–1946. https://doi.org/10.1080/19443994.2013.806224
133. Chen JH, Xing HT, Guo HX, Weng W, Hu SR, Li SX, Huang YH, Sun X, Su ZB (2014) Investigation on the adsorption properties of Cr(VI) ions on a novel graphene oxide (GO) based composite adsorbent. J Mater Chem A 2(31):12561–12570. https://doi.org/10.1039/c4ta02004a
134. Yang H, Sun L, Zhai J, Li H, Zhao Y, Yu H (2014) In situ controllable synthesis of magnetic Prussian blue/graphene oxide nanocomposites for removal of radioactive cesium in water. J Mater Chem A 2(2):326–332. https://doi.org/10.1039/c3ta13548a
135. Cui L, Wang Y, Gao L, Hu L, Yan L, Wei Q, Du B (2015) EDTA functionalized magnetic graphene oxide for removal of Pb(II), Hg(II) and Cu(II) in water treatment: adsorption mechanism and separation property. Chem Eng J 281:1–10. https://doi.org/10.1016/j.cej.2015.06.043
136. Li Q, Yu J, Zhou F, Jiang X (2015) Synthesis and characterization of dithiocarbamate carbon nanotubes for the removal of heavy metal ions from aqueous solutions. Colloids Surf A Physicochem Eng Asp 482:306–314. https://doi.org/10.1016/j.colsurfa.2015.06.034
137. Tan L, Liu Q, Jing X, Liu J, Song D, Hu S, Liu L, Wang J (2015) Removal of uranium(VI) ions from aqueous solution by magnetic cobalt ferrite/multiwalled carbon nanotubes composites. Chem Eng J 273:307–315. https://doi.org/10.1016/j.cej.2015.01.110
138. Xie Y, Huang Q, Liu M, Wang K, Wan Q, Deng F, Lu L, Zhang X, Wei Y (2015) Mussel inspired functionalization of carbon nanotubes for heavy metal ion removal. RSC Adv 5(84):68430–68438. https://doi.org/10.1039/c5ra08908e
139. Zong P, Gou J (2014) Rapid and economical synthesis of magnetic multiwalled carbon nanotube/iron oxide composite and its application in preconcentration of U(VI). J Mol Liq 195:92–98. https://doi.org/10.1016/j.molliq.2014.02.002
140. Xiao D-L, Li H, He H, Lin R, Zuo P-L (2014) Adsorption performance of carboxylated multi-wall carbon nanotube-Fe3O4 magnetic hybrids for Cu(II) in water. New Carbon Materials 29(1):15–25. https://doi.org/10.1016/s1872-5805(14)60122-0
141. Zhou L, Ji L, Ma PC, Shao Y, Zhang H, Gao W, Li Y (2014) Development of carbon nanotubes/CoFe2O4 magnetic hybrid material for removal of tetrabromobisphenol A and Pb(II). J Hazard Mater 265:104–114. https://doi.org/10.1016/j.jhazmat.2013.11.058
142. Sankararamakrishnan N, Jaiswal M, Verma N (2014) Composite nanofloral clusters of carbon nanotubes and activated alumina: an efficient sorbent for heavy metal removal. Chem Eng J 235:1–9. https://doi.org/10.1016/j.cej.2013.08.070
143. Zhao X-H, Jiao F-P, Yu J-G, Xi Y, Jiang X-Y, Chen X-Q (2015) Removal of Cu(II) from aqueous solutions by tartaric acid modified multi-walled carbon nanotubes. Colloids Surf A Physicochem Eng Asp 476:35–41. https://doi.org/10.1016/j.colsurfa.2015.03.016
144. Lasheen MR, El-Sherif IY, Sabry DY, El-Wakeel ST, El-Shahat MF (2013) Removal of heavy metals from aqueous solution by multiwalled carbon nanotubes: equilibrium, isotherms, and kinetics. Desalin Water Treat 53(13):3521–3530. https://doi.org/10.1080/19443994.2013.873880
145. Ruthiraan M, Mubarak NM, Thines RK, Abdullah EC, Sahu JN, Jayakumar NS, Ganesan P (2015) Comparative kinetic study of functionalized carbon nanotubes and magnetic biochar for removal of Cd2+ ions from wastewater. Korean J Chem Eng 32(3):446–457. https://doi.org/10.1007/s11814-014-0260-7

146. Sobhanardakani S, Zandipak R, Fili Z, Ghoochian M, Sahraei R, Farmany A (2015) Removal of V(V) ions from aqueous solutions using oxidized multi-walled carbon nanotubes. J Water Supply Res Technol AQUA 64(4):425–433. https://doi.org/10.2166/aqua.2015.053
147. Mubarak NM, Thines RK, Sajuni NR, Abdullah EC, Sahu JN, Ganesan P, Jayakumar NS (2014) Adsorption of chromium (VI) on functionalized and non-functionalized carbon nanotubes. Korean J Chem Eng 31(9):1582–1591. https://doi.org/10.1007/s11814-014-0101-8
148. Fernando MS, Silva RM, Silva KMN (2015) Synthesis, characterization, and application of nano hydroxyapatite and nanocomposite of hydroxyapatite with granular activated carbon for the removal of Pb2+ from aqueous solutions. Appl Surf Sci 351:95–103. https://doi.org/10.1016/j.apsusc.2015.05.092
149. Azari A, Kakavandi B, Kalantary RR, Ahmadi E, Gholami M, Torkshavand Z, Azizi M (2015) Rapid and efficient magnetically removal of heavy metals by magnetite-activated carbon composite: a statistical design approach. J Porous Mater 22(4):1083–1096. https://doi.org/10.1007/s10934-015-9983-z
150. Zhang H, Huang F, Liu D-L, Shi P (2015) Highly efficient removal of Cr(VI) from wastewater via adsorption with novel magnetic Fe3O4@C@MgAl-layered double-hydroxide. Chin Chem Lett 26(9):1137–1143. https://doi.org/10.1016/j.cclet.2015.05.026
151. Xiong Y, Ye F, Zhang C, Shen S, Su L, Zhao S (2015) Synthesis of magnetic porous γ-Fe2O3/C@HKUST-1 composites for efficient removal of dyes and heavy metal ions from aqueous solution. RSC Adv 5(7):5164–5172. https://doi.org/10.1039/c4ra12468e
152. Zhang Q, Yu G, Wang W-J, Yuan H, Li B-G, Zhu S (2013) Switchable block copolymer surfactants for preparation of reversibly coagulatable and redispersible poly(methyl methacrylate) latexes. Macromolecules 46(4):1261–1267. https://doi.org/10.1021/ma302505r
153. Zhang Q, Yu G, Wang W-J, Li B-G, Zhu S (2012) Preparation of CO2/N2-triggered reversibly coagulatable and redispersible polyacrylate latexes by emulsion polymerization using a polymeric surfactant. Macromol Rapid Commun 33(10):916–921. https://doi.org/10.1002/marc.201200033
154. Lin T, Ma S, Lu Y, Guo B (2014) New design of shape memory polymers based on natural rubber crosslinked via oxa-Michael reaction. ACS Appl Mater Interfaces 6(8):5695–5703. https://doi.org/10.1021/am500236w
155. Yu G, Lu Y, Liu X, Wang W-J, Yang Q, Xing H, Ren Q, Li B-G, Zhu S (2014) Polyethylenimine-assisted extraction of α-tocopherol from tocopherol homologues and CO2-triggered fast recovery of the extractant. Ind Eng Chem Res 53(41):16025–16032. https://doi.org/10.1021/ie502568h
156. Lu Y, Yu G, Wang W-J, Ren Q, Li B-G, Zhu S (2015) Design and synthesis of thermoresponsive ionic liquid polymer in acetonitrile as a reusable extractant for separation of tocopherol homologues. Macromolecules 48(4):915–924. https://doi.org/10.1021/ma502611s
157. Wang W, Zhang Q, Yu G, Li B, Zhu S (2014) Amphiphilic macromolecular emulsifier with switchable surface activity and use thereof in preparation of polymer latex. US Patent 20140316049A1
158. Zhang Q, Yu G, Wang W-J, Yuan H, Li B-G, Zhu S (2012) Preparation of N2/CO2 triggered reversibly coagulatable and redispersible latexes by emulsion polymerization of styrene with a reactive switchable surfactant. Langmuir 28(14):5940–5946. https://doi.org/10.1021/la300051w
159. Yu G (2015) Separation of tocopherol homologues using amino-based polymer extractants. Master's Thesis, Zhejiang University, China
160. Cao Y, Li X (2014) Adsorption of graphene for the removal of inorganic pollutants in water purification: a review. Adsorption 20(5–6):713–727. https://doi.org/10.1007/s10450-014-9615-y
161. Yu J-G, Zhao X-H, Yu L-Y, Jiao F-P, Jiang J-H, Chen X-Q (2013) Removal, recovery and enrichment of metals from aqueous solutions using carbon nanotubes. J Radioanal Nucl Chem 299(3):1155–1163. https://doi.org/10.1007/s10967-013-2818-y
162. Kyzas GZ, Matis KA (2015) Nanoadsorbents for pollutants removal: a review. J Mol Liq 203:159–168. https://doi.org/10.1016/j.molliq.2015.01.004
163. Foo KY, Hameed BH (2010) Insights into the modeling of adsorption isotherm systems. Chem Eng J 156(1):2–10. https://doi.org/10.1016/j.cej.2009.09.013
164. Zhou G, Liu C, Tang Y, Luo S, Zeng Z, Liu Y, Xu R, Chu L (2015) Sponge-like polysiloxane-graphene oxide gel as a highly efficient and renewable adsorbent for lead and cadmium metals removal from wastewater. Chem Eng J 280:275–282. https://doi.org/10.1016/j.cej.2015.06.041
165. Tofighy MA, Mohammadi T (2015) Copper ions removal from water using functionalized carbon nanotubes–mullite composite as adsorbent. Mater Res Bull 68:54–59. https://doi.org/10.1016/j.materresbull.2015.03.017
166. Zhang M-M, Liu Y-G, Li T-T, Xu W-H, Zheng B-H, Tan X-F, Wang H, Guo Y-M, Guo F-Y, Wang S-F (2015) Chitosan modification of magnetic biochar produced from Eichhornia crassipes for enhanced sorption of Cr(VI) from aqueous solution. RSC Adv 5(58):46955–46964. https://doi.org/10.1039/c5ra02388b
167. Tan P, Sun J, Hu Y, Fang Z, Bi Q, Chen Y, Cheng J (2015) Adsorption of Cu2+, Cd2+ and Ni2+ from aqueous single metal solutions on graphene oxide membranes. J Hazard Mater 297:251–260. https://doi.org/10.1016/j.jhazmat.2015.04.068
168. Jahangiri M, Kiani F, Tahermansouri H, Rajabalinezhad A (2015) The removal of lead ions from aqueous solutions by modified multi-walled carbon nanotubes with 1-isatin-3-thiosemicarbazone. J Mol Liq 212:219–226. https://doi.org/10.1016/j.molliq.2015.09.010
169. Wang S, Gao B, Zimmerman AR, Li Y, Ma L, Harris WG, Migliaccio KW (2014) Removal of arsenic by magnetic biochar prepared from pinewood and natural hematite. Bioresour Technol 175:391–395. https://doi.org/10.1016/j.biortech.2014.10.104
170. Chen L, Wang H, Wei H, Guo Z, Khan MA, Young DP, Zhu J (2015) Carbon monolith with embedded mesopores and nanoparticles as a novel adsorbent for water treatment. RSC Adv 5(53):42540–42547. https://doi.org/10.1039/c5ra03014e
171. Hall KR, Eagleton LC, Acrivos A, Vermeulen T (1966) Pore- and solid-diffusion kinetics in fixed-bed adsorption under constant-pattern conditions. Ind Eng Chem Fundamen 5(2):212–223
172. Zheng H, Liu D, Zheng Y, Liang S, Liu Z (2009) Sorption isotherm and kinetic modeling of aniline on Cr-bentonite. J Hazard Mater 167(1–3):141–147. https://doi.org/10.1016/j.jhazmat.2008.12.093
173. Sun C-J, Sun L-Z, Sun X-X (2013) Graphical evaluation of the favorability of adsorption processes by using conditional Langmuir constant. Ind Eng Chem Res 52(39):14251–14260. https://doi.org/10.1021/ie401571p
174. Dada AO, Olalekan AP, Olatunya AM, Dada O (2012) Langmuir, Freundlich, Temkin and Dubinin-Radushkevich isotherms studies of equilibrium sorption of Zn2+ unto phosphoric acid modified rice husk. IOSR Journal of Applied Chemistry 3(1):38–45
175. Gu X, Yang Y, Hu Y, Hu M, Wang C (2015) Fabrication of graphene-based xerogels for removal of heavy metal ions and capacitive deionization. ACS Sustain Chem Eng 3(6):1056–1065. https://doi.org/10.1021/acssuschemeng.5b00193
176. Tofighy MA, Mohammadi T (2014) Synthesis and characterization of ceramic/carbon nanotubes composite adsorptive membrane for copper ion removal from water. Korean J Chem Eng 32(2):292–298. https://doi.org/10.1007/s11814-014-0210-4
177. Liu H, Zhang J, Ngo HH, Guo W, Wu H, Cheng C, Guo Z, Zhang C (2015) Carbohydrate-based activated carbon with high surface acidity and basicity for nickel removal from synthetic wastewater. RSC Adv 5(64):52048–52056. https://doi.org/10.1039/c5ra08987e